Pontificia Universidad Católica del Perú

Escuela de Posgrado

Título

Durability of porous glasses

Tesis para obtener el grado de
Magíster en Ingeniería y Ciencia de los Materiales

Presentado por: Christian Raúl Rodríguez Valdivieso

Tutor Responsable (TU Ilmenau): Prof. Dr.-Ing. Edda Rädlein
Professor Responsable (TU Ilmenau): Dr. Andreas Christian Herrmann
Professor Responsable (PUCP): Dr.-Ing. Rolf Grieseler

Fecha y Lugar: 02/12/2021, Ilmenau

DECLARATION OF AUTONOMY

I hereby declare that I have written this thesis on the subject of "Durability of porous glasses" myself and that I have not used any other sources than those given. All thoughts that have been taken directly or indirectly from external sources are marked as such. The work has not yet been submitted to any other examining authority and has not yet been published.

Ilmenau, 19.11.21

Ort, Datum

Christian Raúl Rodriguez Valdivieso

ABSTRACT

The investigations of this work are dedicated to the production of highly alkali resistant porous glasses, evaluating the effect of adding ZrO_2 to the sodium borosilicate Vycor-type glass. The additions were made with the purpose of improving the ability of the silica porous structure to withstand alkaline solutions. Base glasses (BG) with 0 mol% ZrO_2 (Zr0), 3 mol% ZrO_2 (Zr3) and 6 mol% ZrO_2 (Zr6) were produced by the conventional melting and quenching method. The vitreous structure of the BG was confirmed by XRD. Further characterization tests such as density, ATR and DSC were performed as well. To induce spinodal phase separation and create a two-phase matrix (an insoluble silica rich phase and a soluble sodium-borate phase), BG were heat treated at different temperatures from 560 °C to 700 °C for 12 hours. Scanning electron microscopy (SEM) confirmed the expected interconnected sponge-like morphology. Pore sizes were calculated according to the DIN EN ISO 13383 norm. There is a well-defined tendency of pore size growth with increasing heat treatment temperature and time for 0 mol% ZrO_2 and 3 mol% ZrO_2 glasses. SEM images also show a decrease in pore size when ZrO_2 is added to the glass. The 6 mol% ZrO_2 glass did not show spinodal phase separation.

Based on the pore size results, a heat treatment temperature of 680 °C was chosen for the following tests. To obtain a porous sample, the soluble sodium-borate phase needs to be leached with HCl solution. For this, leaching temperature and the HCl solution were varied, as well as the subsequent drying process.The best leaching results were obtained with a solution of 1 M HCl + 70 % Ethanol (ratio 9:1) at room temperature for two days and 2 M HCl + 70 % Ethanol (ratio 9:1) at 70 °C for seven days, for Zr0 and Zr3, respectively. To study the durability of porous glasses, alkali resistance tests against 0.1 M NaOH were carried out. It was shown that the alkali stability of Zr0 glass is very low (mass loss of about 20 % in 22 hours). However, when 3 mol% ZrO_2 is added to the glass the weight loss percentage is reduced significantly (mass loss of about 4 % in 22 hours). It was found that the presence of zirconia in the silica rich porous structure improves the stability against alkali dramatically. A big problem is the leaching of the phase separated glasses, which very often resulted in breaking of the samples.

RESUMEN

Las investigaciones de este trabajo se basan en la producción de vidrios porosos altamente resistentes a los álcalis, evaluando el efecto de la adición de ZrO_2 al vidrio borosilicato de sodio tipo Vycor. Las adiciones se realizaron con el propósito de mejorar la capacidad de la estructura porosa de sílice para resistir soluciones alcalinas. Se produjeron vidrios base (BG) de 0 % mol ZrO_2 (Zr0), 3 % mol ZrO_2 (Zr3), 6 % mol ZrO_2 (Zr6) mediante el método convencional de fusión y enfriamiento. La estructura amorfa de BG fue confirmada por DRX. También se realizaron más pruebas de caracterización como densidad, ATR y DSC. Para inducir la separación de fases espinodal y crear una matriz de dos fases (una fase insoluble rica en sílice y una fase soluble de borato de sodio), se trataron térmicamente BG a diferentes temperaturas de 560 °C a 700 °C durante 12 horas. La microscopía electrónica de barrido (SEM) confirmó la morfología esperada similar a una esponja interconectada. Los tamaños de los poros se calcularon según la norma DIN EN ISO 13383. Existe una tendencia bien definida de crecimiento del tamaño de los poros con el aumento de la temperatura y el tiempo del tratamiento térmico para vidrios con 0 % mol ZrO2 y 3 % mol ZrO2. Las imágenes SEM también muestran una disminución en el tamaño de los poros cuando se agrega ZrO_2 al vidrio. El vidrio de ZrO_2 al 6 % en moles no mostró separación de fases espinodal.

Basándose en los resultados del tamaño de los poros, se eligió una temperatura de tratamiento térmico de 680 °C para las siguientes pruebas. Para obtener una muestra porosa, la fase soluble de borato de sodio debe lixiviarse con una solución de HCl. Para ello se varió la temperatura de lixiviación y la solución de HCl, así como el posterior proceso de secado, los mejores resultados de lixiviación se obtuvieron con una solución de 1 M HCl + Etanol al 70 % (proporción 9: 1) a temperatura ambiente durante dos días y 2 M HCl + etanol al 70 % (proporción 9: 1) a 70 °C durante siete días, para Zr0 y Zr3, respectivamente. Para estudiar la durabilidad de los vidrios porosos, se llevaron a cabo pruebas de resistencia a los álcalis frente a 0.1 M NaOH. Se demostró que la estabilidad alcalina del vidrio Zr0 es muy baja (pérdida de masa de aproximadamente el 20 % en 22 horas). Sin embargo, si se añade al vidrio un 3 % en moles de ZrO_2, el porcentaje de pérdida de peso se reduce significativamente (pérdida de masa de aproximadamente 4 % en 22 horas). Se encontró que la presencia de zirconia en la estructura porosa rica en sílice mejora la estabilidad frente a los álcalis drásticamente. Un gran problema es la lixiviación de los vidrios con separación de fases, que muy a menudo provoca la rotura de las muestras.

ZUSAMMENFASSUNG

In dieser Arbeit sollten hoch alkalibeständige poröse Gläser hergestellt werden, wobei die Wirkung der Zugabe von ZrO2 zu einem Natriumborsilikatglas vom Vycor-Typ untersucht wurde. Der ZrO2 Zusatz wurden mit dem Ziel vorgenommen, die Fähigkeit der porösen Siliciumdioxidstruktur zu verbessern, alkalischen Lösungen zu widerstehen. Basisgläser mit 0 mol% ZrO2 (Zr0), 3 mol% ZrO2 (Zr3) und 6 mol% ZrO2 (Zr6) wurden durch das herkömmliche Schmelzverfahren hergestellt. Die amorphe Struktur der Basisgläser wurde durch XRD bestätigt. Weitere Charakterisierungen wie Dichte, ATR und DSC wurden ebenfalls durchgeführt. Um eine spinodale Phasentrennung zu induzieren und eine zweiphasige Matrix (eine unlösliche silikatreiche Phase und eine lösliche Natriumborat-Phase) zu erzeugen, wurden die Basisgläser 12 Stunden lang bei unterschiedlichen Temperaturen von 560 °C bis 700 °C wärmebehandelt. Rasterelektronenmikroskopische Aufnahmen (REM) bestätigten die erwartete Durchdringungsstruktur. Porengrößen wurden nach der Norm DIN EN ISO 13383 berechnet. Bei Gläsern mit 0 mol% ZrO2 und 3 mol% ZrO2 besteht eine wohldefinierte Tendenz zum Porengrößenwachstum mit zunehmender Wärmebehandlungstemperatur und -zeit. REM-Bilder zeigen eine Abnahme der Porengröße, wenn ZrO2 zum Glas hinzugefügt wird. Das 6 mol% ZrO2-Glas zeigte keine spinodale Phasentrennung.

Basierend auf den Ergebnissen der Porengrößenmessung wurde für die folgenden Tests eine Wärmebehandlungstemperatur von 680 °C gewählt. Um eine poröse Probe zu erhalten, muss die lösliche Natriumborat-Phase mit HCl-Lösung ausgelaugt werden. Dazu wurden Temperatur und HCl-Lösung sowie der anschließende Trocknungsprozess variiert. Die besten Auslaugungsergebnisse wurden mit einer Lösung aus 1 M HCl + 70% Ethanol (Verhältnis 9:1) bei Raumtemperatur für zwei Tage (Zr0) und 2 M HCl + 70% Ethanol (Verhältnis 9:1) 70 °C für sieben Tage (Zr3) erzielt. Um die Alkalistabilität der porösen Gläser zu untersuchen, wurden Löslichkeitstests gegen 0,1 M NaOH durchgeführt. Es zeigte sich, dass die Alkalistabilität von Zr0 sehr gering ist (Massenverlust von ca. 20 % in 22 Stunden). Wenn dem Glas jedoch 3 mol% ZrO2 hinzugefügt werden, wird der Gewichtsverlust signifikant verringert (Massenverlust von etwa 4% in 22 Stunden). Es wurde festgestellt, dass die Anwesenheit von Zirkoniumdioxid in der silikatreichen porösen Glasmatrix die Stabilität gegenüber Alkalilösungen maßgeblich verbessert. Ein großes Problem stellt jedoch das Auslaugen der phasenseparierten Gläser dar. Dies führt sehr oft zum Zerbrechen der Glassamples.

ACKNOWLEDGEMENTS

I would like to express my sincere gratitude to my supervisor, in TU Ilmeanu, Prof. Rädlein for presenting this topic to me and giving insights for the development of this research. I am very much grateful to Dr. Andreas Herrmann, without his continuous support and guidance throughout these months this work would have not been possible.

I would also like to thank my supervisor Dr. Rolf Grieseler from Pontificia Universidad Católica del Perú for the opportunity to do the double degree program here in Germany and for the constant advice during my research.

I wish to thank my parents, Patricia Valdivieso and Oscar Rodríguez. I am forever indebted for their love, constant encouragement and support during all these years, particularly during these months away from home.

TABLE OF CONTENTS

List of figures

List of tables

Abbreviations

BG	Base glass
CN	Coordination number
Zr0-BG	0 mol% ZrO_2 glass
Zr3-BG	3 mol% ZrO_2 glass
Zr6-BG	6 mol% ZrO_2 glass
XRD	X-ray diffraction
SEM	Scanning electron microscopy
Zr0-680	0 mol% ZrO_2 glass heat treated at 680°C
Zr3-680	3 mol% ZrO_2 glass heat treated at 680°C
RO	Reverse osmosis
MF	Micro filtration
NF	Nano filtration
UF	Ultrafiltration
PG	Porous glass
T_m	Melting temperature
T_f	Fictive temperature
T_g	Glass transition temperature
BO	Bridging oxygen
NBO	Non-bridging oxygen
RT	Room temperature

CHAPTER 1

1. Motivation

The research and continuous development of nanotechnology in today's world, particularly in nanostructured materials, has been of great impact in recent decades. Nano-porous materials are becoming more important than ever as they present significant potential for a new generation of functional materials which can be used in different industrial fields such as filtration, energy storage, sensors, catalysis, etc. [1][2].

Membrane separation technologies such as reverse osmosis (RO), microfiltration (MF), nano-filtration (NF), ultrafiltration (UF) are some of the most-well known and remarkable membrane based technologies for separation of waste effluents, salts, enzymes, proteins, etc. compared to other technologies (oxidation, photo-catalysis, adsorption, electrochemistry) [3-6].

However, they present a major drawback called fouling. A rapid and sometimes irreversible loss of flux in operation is caused by the interaction between different elements present in water and the porous membrane [4][7].

Ever since the discovery of porous glasses (PG) fabrication in the sodium borosilicate glass system, a fast-growing research area was developed. Porous glasses can be used successfully in membrane separation processes as they exhibit controlled pore sizes, pore volume and surface area for different applications, as well as higher mechanical, thermal, chemical stability than other organic network membranes [8][9].

For industrial applications sodium hydroxide stability is required, as alkaline solutions are optimal for sanitation and cleaning of different components, especially in separation processes [10-15].

As it has been stated in several studies, unfortunately NaOH solutions tend to react with silica by breaking down silica and silicon oxygen radicals in the glass structure [16-18]. Increasing the alkali stability of porous glass against NaOH will help position PG as a better candidate for separation technologies. This research aims to evaluate the phase separation and durability of porous glass when zirconia is added to a phase separating glass composition.

CHAPTER 2

2. Literature review

2.1. Definition of glass

Glass has played an important role in the development of society, as it is known, so much that it is plausible to believe we are living in the “glass age” [19].

For decades, researchers have struggled to come up with a specific definition of glass given its complexity as it exhibits solid and liquid features but also unique characteristics. Traditionally glass is made by a melting process, however melting is not a strict requirement to produce glass since there are other technologies such as sol-gel, vapor deposition, etc. [20].

Studies have proven glass to be amorphous and glass presents a thermal characteristic called “glass transition” [21].

A more elaborate and detailed description for glasses is the following: “Glass is a non-equilibrium, non-crystalline condensed state of matter, lacking in long range, periodic atomic structure that exhibits a region of glass transformation behavior” [19][22].

For a better understanding of the glass nature, it is better to comprehend the enthalpy vs. temperature diagram (see Figure 2.1). Above the melting point (T_m), all liquids are thermodynamically stable. Normally, when cooling a melt below T_m crystallization occurs with a drastical decrease of the enthalpy. However, if cooling can be carried out without crystallization a metastable supercooled liquid is formed which will tend to crystallize if a thermodynamic barrier is overcome. As temperature decreases, the viscosity increases until it becomes so high that atom arrangement is blocked and is no longer temperature dependent. As stated by Shelby “The temperature region laying between the limits where the enthalpy is that of the equilibrium and that of the frozen solid, is known as the glass transformation region. The frozen liquid is now a glass”. It is at this temperature where the slope in Figure 2.1 changes [19][21]. At slower cooling rates the glass transition region shifts to lower temperatures. The fictive temperature (T_f) allows to distinguish the difference in the thermal history of these glasses (fast and slow cooled). At this temperature the glass structure is considered to be that of the equilibrium liquid [20].

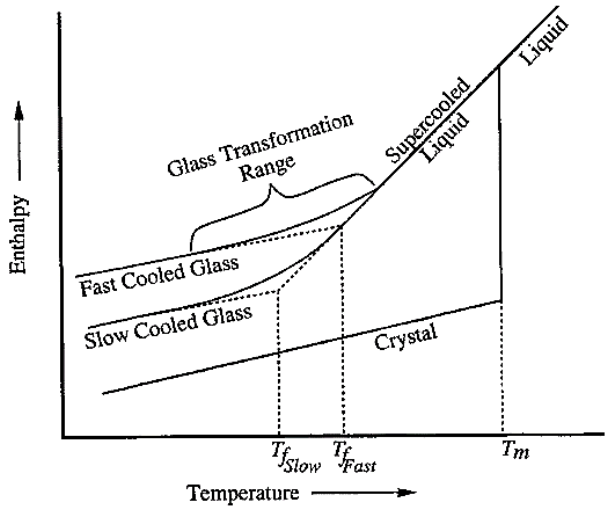

Figure 2.1: Effect of temperature on glass enthalpy. Slower cooling rates move the glass transition region to lower temperatures and decrease the fictive temperature (T_f) [20].

2.2. Random network of glasses

There have been several models proposed to describe the structure of glass. In 1932 Zachariasen [23], defined a condition for glass formation as: "a substance can form extended three-dimensional networks lacking periodicity with an energy content comparable with that of the corresponding crystal network."

The glass forming ability of oxide network formers (SiO_2, B_2O_3, P_2O_5) can be affected with the addition of alkali oxides by network modification (see Figure 2.2) [21]. With this in consideration, Zachariasen postulated three rules for oxide glass formation [23].

- A high percentage of network forming cations are surrounded by oxygen tetrahedra or oxygen triangles.
- The oxygen tetrahedra or triangles only share corners with each other.
- Oxygen atoms are linked to only two cations, and new bonds with other cations are not formed.

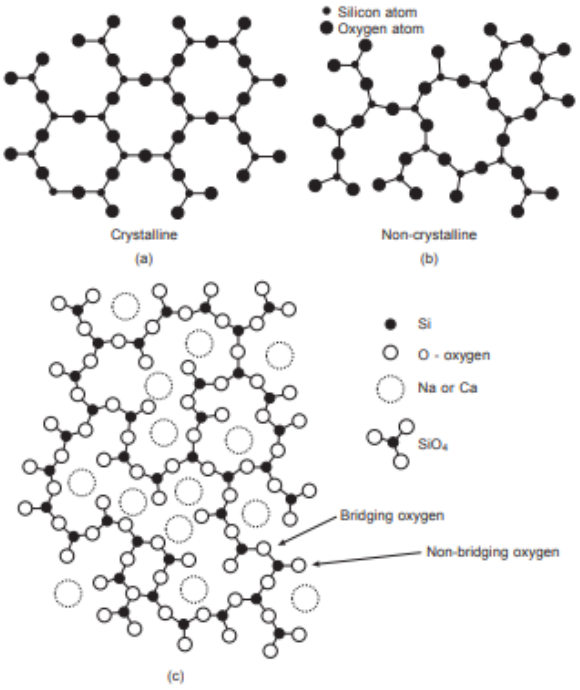

Figure 2.2: Schematic structure representation of a) quartz, b) silica glass and c) soda lime silicate glass. Note that the fourth oxygen atom of the SiO_4 tetrahedra is situated below or above the figure plane and not drawn [24].

Zachariasen classified cations as network formers, e.g. Si^{4+}, which can create a three dimensional network of tetrahedral $[SiO_{4/2}]^0$ units neutrally charged with all of the 4 oxygen corners being shared. The network contains Si-O-Si bonds, however, in the presence of an alkali oxide (network modifier) depolymerization occurs, the Si-O-Si bonds break to form $Si\text{-}O^-$ terminations opening up the 3-D structure.

The oxygen in Si-O-Si is called “bridging oxygen” (BO) and the one in $Si\text{-}O^-$ is known as “non-bridging oxygen” (NBO) (see Figure 2.3) [20],[23-25].

$$\equiv Si\text{-}O\text{-}Si \equiv + Na_2O = 2Si\text{-}O^- + 2Na^+ + \tfrac{1}{2}O_2$$

In the silicate glass depolymerized network, which consists of several NBO and BO, the term Q^n (see Figure 2.3) is used to denote the Si environment where n varies from 0 to 4 and indicates the number of BO [26][27].

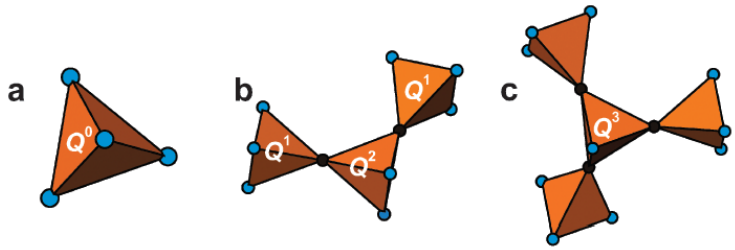

Figure 2.3: Q^n nomenclature illustration. Non-bridging in blue and bridging oxygen in black. a) Q^0 tetrahedron , b) Q^2 unit bonded with two Q^1 units, c) Q^3 connected to three Q^1 units [28].

Network intermediates can either reinforce the glass structure as forming units, with a coordination number (CN) of 4, or loosen the structure as network modifiers (CN of 6-8), but are unable to form glasses alone [29]. The addition of large cations in the glass network creates broken bonds, consequently there is an increase of the network units mobility generating lower viscosity, lower melting temperature and increase in electrical conductivity [30].

2.3. Borosilicate glass

For several years, borosilicate glasses have been of great commercial and technological importance because of their specialized applications. During melting of glass, the addition of boron provides lower melting temperatures, better dissolution of raw materials (flux agent), lower viscosity, inhibition of devitrification [31].

Borosilicate glasses generally exhibit a higher thermal shock resistance (higher than soda-lime silica glasses), excellent chemical resistance against most acids, high dielectric strength and higher softening temperature compared to soda-lime silica glasses. Therefore, they are used for laboratory glassware, household cooking ware, lamps, radioactive waste glasses, etc. [32]. These properties vary depending on the SiO_2/B_2O_3 ratio [30][33][34].

Raman spectroscopy and NMR studies have provided a great amount of useful information of the different unit structures present in the glass network, as well as of BO and NBO. In borosilicate glasses, three-fold coordinated boron [BO_3] and four-fold coordinated boron $[BO_4]^-$ units have been found [35].

However additional superstructures are present as well, reedmergerite-like (see Figure 2.4a), a $[BO_4]^-$ tetrahedron surrounded by four $[SiO_4]$ tetrahedra, and danburite-like superstructures (see Figure 2.4b), a ring of two $[SiO_4]$ and two $[BO_4]^-$ tetrahedra. The negative charges of the $[BO_4]^-$ groups are compensated by the network modifying cations, in the glasses as well as in the crystals [34][35].

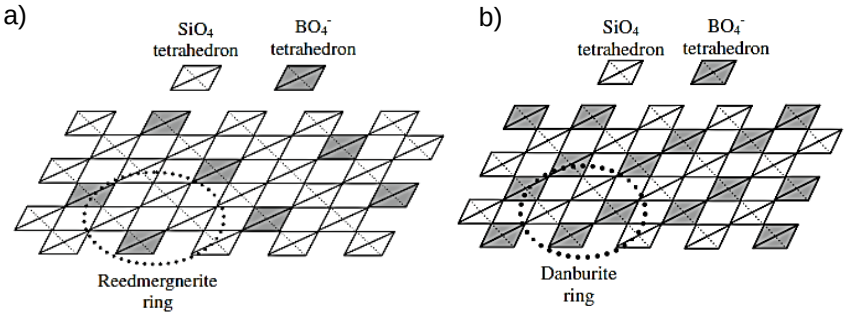

Figure 2.4: Schematic structure of a) reedmergerite $NaSi_3BO_8$ and b) danburite $Ca[B_2Si_2O_8]$ [36].

2.4. Porous material

Porous ceramics are essential engineering materials due to their high demand in different industrial fields depending on the pore characteristics. Porous materials microstructure and properties depend on the process used. In the last decade, increasing research has been dedicated to processing technologies in order to control porous structures and to improve general properties. Making a dense material porous provides new, useful properties to certain applications that dense materials are not suited for. High surface area, high permeability, high porosity, low specific heat and high thermal insulation are common properties of porous materials [37].

Pores are considered one of the most relevant features of a material, its connectivity and pore size are fundamental for transport in porous materials. The pore shape, pore strut/wall size and shape, surface roughness, and surface area play also an important role in final properties [36][37].

There are many applications for porous materials due to their excellent overall performance. The ultimate goal for the development of these materials and the characterization of their properties is to use them to meet specific design requirements.

The physical properties demonstrated by these materials are a reflection of the internal structure, so in order to improve them, their internal structures need to be understood correctly [38].

It is difficult to determine a general and comprehensive classification of pores. However, a proper way to classify them is by the accessibility of an external material or fluid to get into the inner structure [39].

Figure 2.5 represents the different types of pores. Pores (b), (c), (d), (e) and (f) are open pores because of the interaction with external surface. However, pore (a) is a closed one and these pore are important for bulk density, mechanical properties and thermal conductivity [40].

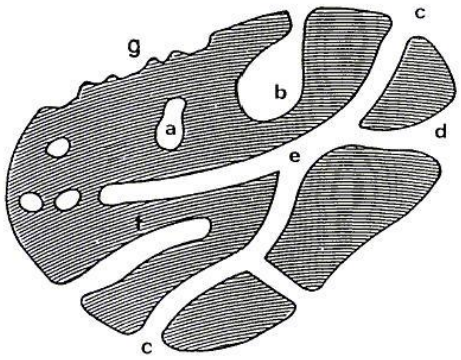

Figure 2.5: Schematic cross-section of a porous solid, (a) closed pore and (b)-(f) open pores [40].

According to the nomenclature of IUPAC (International Union of Pure and Applied Chemistry), porous materials are classified depending on the pore diameter as shown in Table 2.1 [41].

Table 2.1: Classification of porous materials regarding their pore width [41].

Pore type	**Pore width (nm)**
Microporous	< 2
Mesoporous	2-50
Macroporous	> 50

2.5. Porous glass

High silica porous glass has gained interest in recent decades because of its potential use in a variety of applications and basic research. As a general agreement, porous glasses have similar physical behaviors to non-porous glasses which can vary depending on the porosity [42] and even be superior to porous polymeric and ceramic materials [43].

Large surface area, controllable pore size, mechanical stability, high temperature resistance are properties that motivated research with the intention of finding applications in sensors [44-46], batteries [47-49], membrane [50-52] and catalytic technology [53-55].

Porous glass of the borosilicate system was patented by Hood and Nordberg in 1938 and it was not until the 1970s that Vycor® glass was developed [56]. Vycor® is based on a matrix consisting of 96-98 % of a porous, rigid, sponge-like SiO_2 framework that can be filled with different materials and may contain cristobalite phases on the pore surface and/or finely dispersed SiO_2 in the pores [57][58].

Similar to conventional glasses, porous glasses can be produced in various binder-free geometric shapes such as granulates, beads, plates, sticks, tubes, fibers [59].

Vycor® glass membranes have been extensively studied for membrane technologies including nano and ultra-filtration, gas separation [50][60][61]. In the manufacturing process of a Vycor® glass, a specific borosilicate glass plays a significant role. It is produced by using a phase separation phenomenon [62] (to be discussed in section 2.7). Vycor® is a good alternative for fused silica because it can be produced at much lower temperatures and in almost any shape [63].

However, it has low a chemical durability against alkali solutions because of its high silica content [64]. Against alkali solutions, the porous silica network is slowly weakened by the attack of OH^- ions which break the Si-O bonds. Consequently, glass dissolution occurs along with an increase in pore size of the porous structure. Vycor® glass also is soluble in water at room temperature (100 g/m^{-3}). Therefore, membranes for aqueous solutions have limited use [43].

2.6. Boron anomaly

When a network modifier is added to a silicate glass, the Si-O-Si bonds are broken and non-bridging oxygen (NBO) sites $Si\text{-}O^-$ are formed and the network is depolymerized. The NBO sites are needed for charge compensation of the network modifying cations. Therefore, a change in properties is detected. In borate glasses a different structural change occurs. Given the small size of the boron ion, it forms trigonal [BO_3] units. A boroxol ring is considered the main constituent of borate glasses. It consists of 3 [BO_3] (six B-O bonds). In presence of alkali, [BO_3] is transformed to $[BO_4]^-$ by the reaction of O^{2-} with two trigonal borons [21].

The boron coordination number increases from 3 to 4 instead of the formation of non-bridging oxygen at the BO_3 triangles ($BO_3 \rightarrow BO_4^-$ tetrahedra). This change in CN is often called speciation and its defined by: $2\,[BO_3] + Na_2O + ½\,O_2 = 2\,[BO_4]^- + 2\,Na^+$ [32].

In borate glasses, small additions of alkali oxides tend to decrease the coefficient of thermal expansion (formation of $[BO_4]^-$ units, hence promoting network polymerization) but increase at higher amounts of alkali oxide (for Na_2O at about 16 mol%) (decrease in $[BO_4]^-$ units and formation of NBO, depolymerization) [65][66]. The amount of BO_4 units goes to zero in the composition range about (65-75 mol%) [67]. This behavior is called “the Boron anomaly” and also contributes to glass phase separation in borosilicate glasses (see Figure 2.6) [68]. The glass structure is strongly influenced by the change in the boron coordination when alkali ions are added [32].

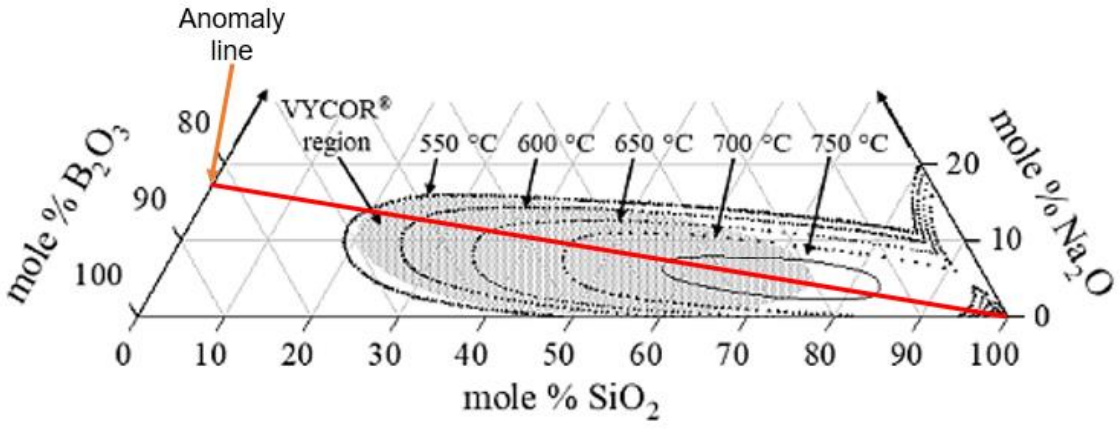

Figure 2.6: Boron anomaly line at a molar ratio of 16 Na_2O : 84 B_2O_3 and the phase separation region in borosilicate glasses [69].

2.7. Phase separation

The phase separation phenomenon in many cases is a problem in glass production because it tends to modify the homogeneity and properties of the molten glass decreasing its final quality [68]. Glassmakers have only started to apply chemistry and thermodynamics to develop a relationship between vitrification, chemical composition and physical properties since the beginning of the 20th century [70]. Phase separation will occur if the free energy of the two phase system is lower compared to the one of the single phase [71]. Varying the composition of the glass and the heat treatment parameters (temperature and time), glass can exhibit phase separation by two well-known mechanisms: Binodal nucleation and growth and spinodal phase separation. Figure 2.7 shows the immiscibility gap for a sodium silicate system and the structure developed by these mechanisms.

For binodal nucleation and growth, which lays in the metastable region, spherical droplets in a matrix of the second phase are observed. The phase separation is not stable to small variations of composition but will stabilize at higher changes of compositions. After nucleation randomly takes place, the nuclei increase their size by diffusion and coalescence [70][72].

Spinodal phase separation occurs within an unstable region and is characterized by an interconnected two phase structure. It starts with small fluctuations in composition, which with enough time will grow spontaneously and create two interconnected phases. This will lower the free energy of the system until an equilibrium is reached. The phases will increase in size with higher temperatures until a critical point is reached where no phase separation occurs. A borosilicate glass that goes through spinodal phase separation will separate into a silica rich phase and an alkali-borate rich phase. This process is believed to be controlled by the movement of the slowest species (most likely oxygen) [71][72]. The alkali-borate rich phase can be leached out by acid to create an interconnected porous glass [70][73][74].

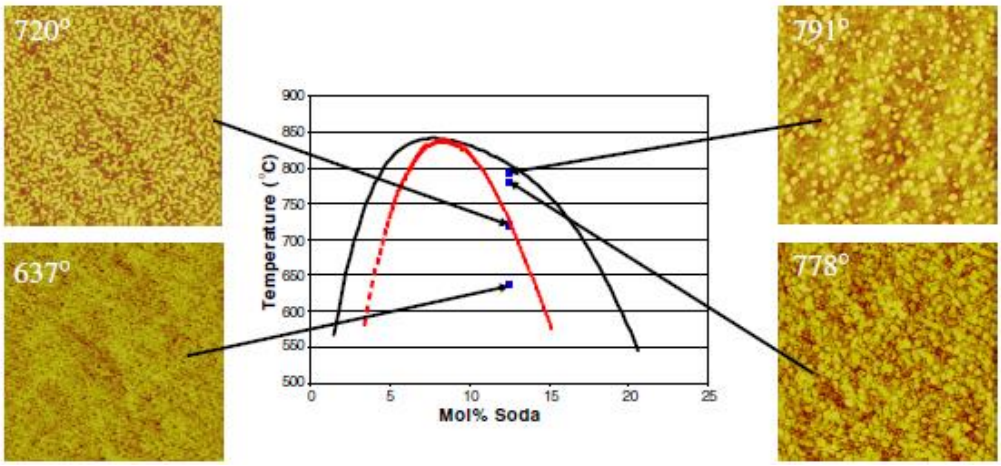

Figure 2.7: Immiscibility diagram of a sodium silicate glass (12.5 Na_2O- 87.5 SiO_2) heat treated for 15 minutes at 637, 720, 778 and 791 °C. Different morphologies measured by AFM are displayed. All AFM images are 3.2 x 3.2 µm. [71].

2.8. Thermodynamics of phase separation

Glass phase separation is very similar to that of liquids. In terms of energy, the free energy of mixing, Δ*Gm*, is denoted by Eq. 1. Two immiscible liquid regions appear if a positive deviation from the ideal condition exists [70][73][74].

$$\Delta G_m = \Delta H_m - T\Delta S_m \qquad \text{(Eq. 1)}$$

ΔH_m is the enthalpy of mixing and ΔS_m the entropy of mixing. In an ideal solution of two components A and B, volume variation (same heterogeneous and homogeneous atom interactions) and the enthalpy of mixing are zero. Therefore, the free energy of mixing depends on the composition (ΔS_m).

$$\Delta G_m = - T\,\Delta S_m \qquad \text{(Eq. 2)}$$

$$\Delta S_m = - R\,[X_A \ln X_A + X_B \ln X_B] \qquad \text{(Eq. 3)}$$

Where X_A and X_B are the components mole fraction and R is the gas constant. Even with variations in the composition, the solution will remain stable if the free energy of mixing is lower compared to the values of the pure components (see Figure 2.8a). However, liquids and glasses don't behave as ideal solutions.

The deviation from ideality and its relation with phase separation can be explained by the enthalpy of mixing, which considers the interaction force Λ between the solution components (Eq. 4 and Eq. 5) [70].

$$\Delta H_m = \Lambda X_A X_B \qquad \text{(Eq. 4)}$$

$$\Lambda = Z N_A (E_{AB} - \frac{1}{2}(E_{AA}+E_{BB})) \qquad \text{(Eq. 5)}$$

Where Z is the components atom coordination number, N_A is Avogadro's number, E_{AB} / E_{AA} / E_{BB} are the interaction energies between the atoms. If Λ is negative, and hence $\Delta H_m<0$ (exothermic process), miscibility of the components occurs. If Λ is positive, and hence $\Delta H_m>0$ (endothermic process), the solution is unstable and demixing of the components (phase separation) proceeds as seen in Figure 2.8b. The following equation describes the phase separation phenomena in a non-ideal solution (Eq. 6) [70].

$$\Delta G_m = \Lambda X_A X_B + RT [X_A \ln X_A + X_B \ln X_B] \qquad \text{(Eq. 6)}$$

If $\Delta H_m>0$ is slightly positive, the solution is still stable and ΔG_m remains negative throughout the compositional range since the entropy term $T\Delta S_m$ is predominant (see Figure 2.8c) [70].

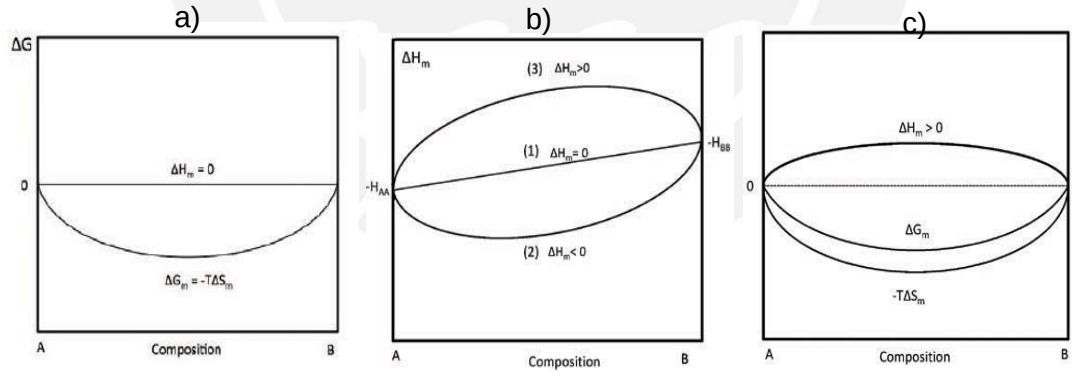

Figure 2.8: a) Variation of free energy of mixing in an ideal solution b) deviation of enthalpy of mixing from ideality c) variation of free energy of mixing with a positive deviation from ideality of the enthalpy [70].

At higher values of $\Delta H_m>>0$, the solution becomes unstable. Temperature plays an important role. At lower temperatures (T1, T3 in Figure 2.9a, b), the entropy term decreases and the enthalpy term becomes significant (see Figure 2.9a, b) showing immiscibility behavior with two minima of ΔG_m.

At higher temperatures the entropy term $T\Delta S_m$ defines the free energy of mixing (see Figure 2.9c) creating unique minima of ΔG_m (miscibility) [70].

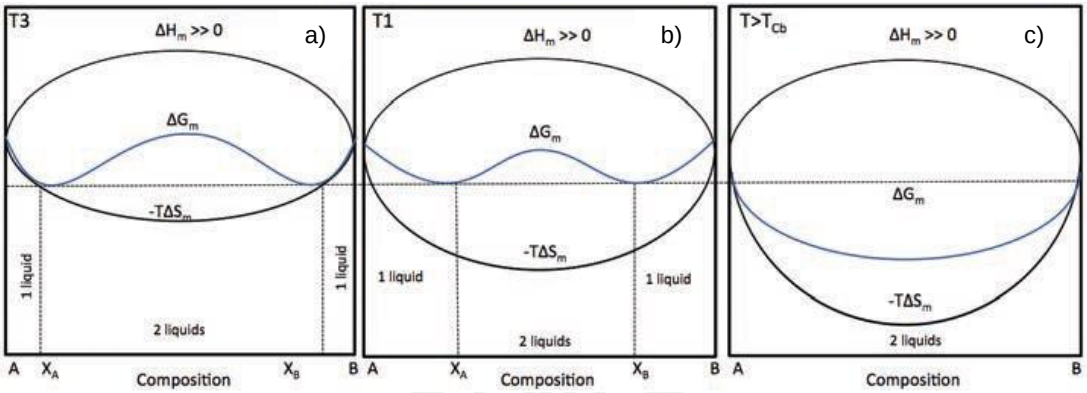

Figure 2.9: Influence of temperature on ΔG_m. a), b) for lower temperatures c) high temperatures [70].

Figure 2.10a shows how thermodynamics has an influence on the phase diagram (immiscibility dome). The position of the spinodal varies at different temperatures. Figure 2.10b allows to understand better the composition fluctuations in phase separation. In point 2 of Figure 2.10b (inside the spinodal region), the composition tends to vary to 2' and 2". Since more energy is withdrawn to generate 2" than spent to reach 2', the total system energy decreases and the fluctuations will be enhanced. This does not happen at point 3. Fluctuation at 3' and 3" are not energetically favorable, thus they disappear [2].

The regions of the dome are separated at point 1, where the slope of the curve changes. In terms of the second derivative of free energy ($\frac{\partial^2 G}{\partial X^2}$) versus the composition at constant pressure and temperature, the regions can be described as follows [2][58]:

Stable region	$\frac{\partial^2 G}{\partial X^2} > 0$
Spinodal points	$\frac{\partial^2 G}{\partial X^2} = 0$
Unstable / metastable region	$\frac{\partial^2 G}{\partial X^2} < 0$

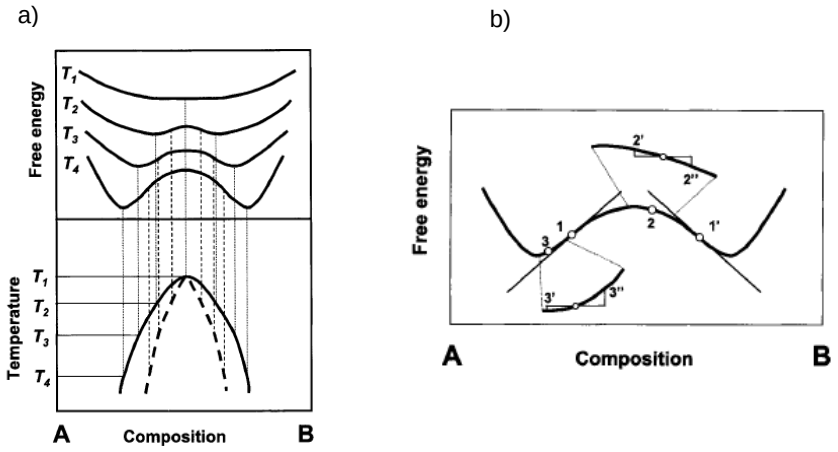

Figure 2.10: a) Phase diagram of the immiscibility dome (solid line) and the spinodal region (dashed line), b) enlarged drawing of an energy curve. Points 1 and 1" are the spinodal points $\frac{\partial^2 G}{\partial X^2} = 0$ and points 2', 2", 3' and 3" indicate compositional fluctuations [2].

2.9. Kinetics of phase separation

In the binodal mechanism (drop-shaped precipitations), elements need to pass through the depletion area following the concentration gradient cancelling the fluctuations (B). This is known as "downhill diffusion". As fluctuations increase to reach equilibrium, this matter supply ends with a nucleus formation of critical size that shows an unchanged composition which will remain the same even with growing size. (see Figure 2.11a). For the spinodal mechanism, the matter supply diffuses against its own concentration until it reaches the equilibrium. This is known as "uphill diffusion" (see Figure 2.11b) [2][74].

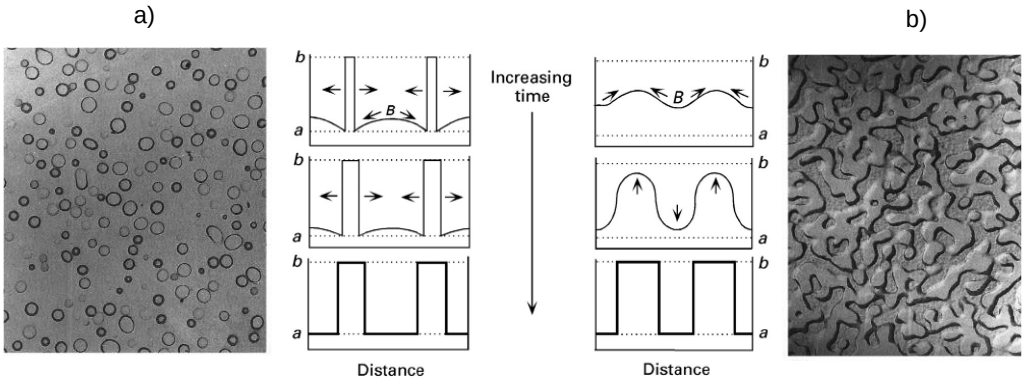

Figure 2.11: Schematic representation of the a) downhill (bimodal) nucleation and growth and b) uphill (spinodal) diffusion [74].

2.10. Influence of heat treatment on the porous structure

Features as pore volume, pore size distribution and morphology are strongly influenced by the initial composition of the glass (e.g. ratio of B_2O_3/Na_2O) but also the heat treatment time and temperature. Since these parameters can be controlled, different properties can be obtained for porous glass after the leaching process [75]. Heat treatment temperatures could range between 400 and 950 °C for 2 hours up to 4 weeks [76].

According to Zhou et al., for $7Na_2O$-$23B_2O_3$-$70SiO_2$ glass, the proper temperature to have an amorphous state and avoid crystallization ranges between 640-680 °C [77]. In the patent US 3549524, Haller, to fabricate membranes for chromatography applications, created a graph (see Figure 2.12) showing the relationship between the heat treatment temperature and the pore size.

This relationship can be described by the Eq. 7 [76]:

$$r^n = kte^{-m/T} \qquad \text{(Eq. 7)}$$

Where:

r : pore radius (Å)
n, k, m : constants
T: temperature (K)
t : time (h)

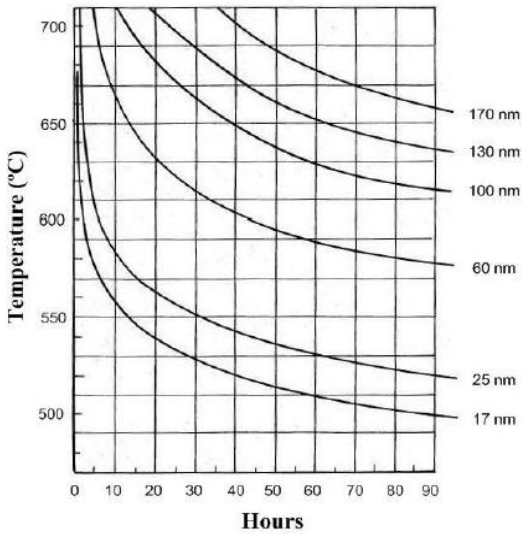

Figure 2.12: Dependence of pore size on heat treatment temperature and time of an alkali borosilicate glass [76].

Evaluating the immiscibility dome of the borosilicate glass system for a molar Na_2O/B_2O_3 ratio of 16/84 in Figure 2.13, the shape of the curve on the right side denotes low values of solubility of the alkali-borate phase in the silica phase. On the other hand, the shape in general confirms an increase in solubility of the silica phase in alkali-borate phase with higher temperatures.

At a fixed temperature, if the composition changes (decreasing the silica content), the alkali-borate phase volume will increase. Therefore, after leaching, higher pore volume will be observed. An increase in temperature (within the dome) will result in a smaller compositional range where phase separation occurs [74][78].

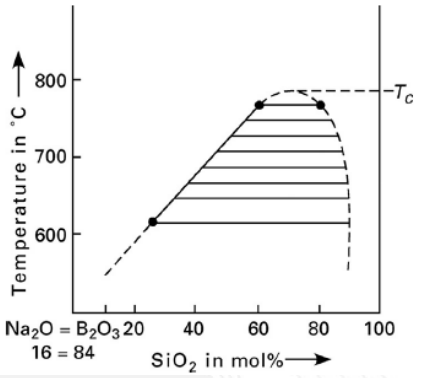

Figure 2.13: Asymmetric immiscibility dome for a $Na_2O–B_2O_3–SiO_2$ glass at a molar Na_2O/B_2O_3 ratio of 16/84 [74].

2.11. Colloidal silica

Back in the 1950s, the presence of colloidal silica, also known as silica gel in porous glasses was postulated [79]. Further research allowed to detect silica gel with various techniques [80-82] and to characterize its structure and texture [83]. Kreisberg et al. detailed the mechanism of silica gel formation (see Figure 2.14) [84]. At the beginning of the acid leaching process, the silica concentration present in the soluble phase is dissolved. However, as the concentration of silica increases in the solution ($Si(OH)_4$), the silica gel coagulates [85]. There is precipitation of the silica on the pore walls which is difficult to leach due its low solubility in acids [86].

Alkaline leaching is used to remove the remaining silica gel from the porous glass. This process can create a bigger pore size and volume [79]. A careful choice of alkaline leaching parameters is needed for a complete extraction of silica gel and to avoid the attack of the porous silica matrix [84][87].

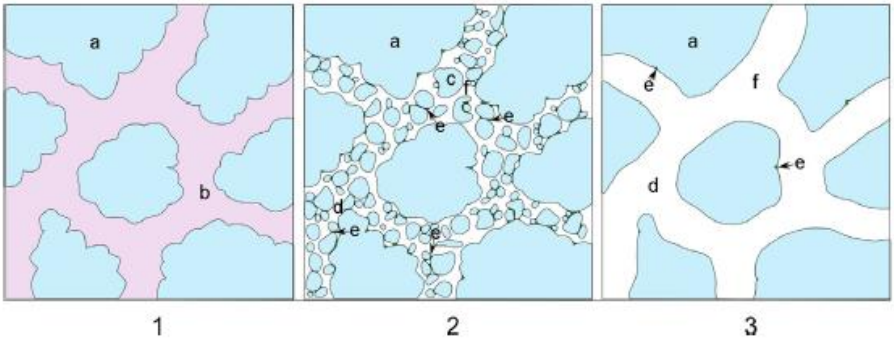

Figure 2.14: Leaching mechanism at different stages. 1) glass after phase separation with a silica rich phase (blue) (a) and an alkali-borate rich phase (pink) (b), 2) porous glass with silica gel (c) in the pore channels (d), 3) porous glass after alkali leaching with pore channels free of silica gel (d and f). Contact points between silica gel and pore walls (e) [84].

2.12. Leaching mechanism

After phase separation, the soluble alkali-borate rich phase is removed from the glass network by a leaching process. The corrosion behavior of glass is suggested as follows [88-90]:

1. The process begins with the interaction of the proton (H^+) or hydronium (H_3O^+) from the water (also aqueous solutions) with the glass matrix which replaces an alkali ion (ion exchange mechanism) which is released into the solution.
   The acidic attack is high at the beginning of the process, with increasing time the leaching rate decreases due to a change in the solution pH as it becomes neutral with the concentration of alkali ions increasing in the solution.
   $$\equiv Si\text{-}O\text{-}R + H_2O \leftrightarrow \equiv Si\text{-}OH + R^+OH^-$$
   Here R is the glass network modifier cation.

2. Further reactions occur between the released hydroxyl and silica.
   $$\equiv Si\text{-}O\text{-}Si\equiv + OH^- \leftrightarrow \equiv Si\text{-}OH + \equiv Si^+\text{-}O^-$$

3. Non-bridging oxygen react with water to produce a hydroxyl ion that will react again over time to continue the dissolution process.
   $$\equiv Si^+\text{-}O^- + H_2O \leftrightarrow \equiv Si\text{-}OH + OH^-$$
4. The alkali borate phase reacts with a proton by an ion exchange mechanism

$$Si\text{-}O^-\text{-}BO_4^- + Na^+ + H^+ \rightarrow Si\text{-}OH + BO_3 + Na^+$$

Different solutions are used for leaching purposes. In the case of distilled water, a small amount of mass loss is detected. H_2O is weakly ionized and the leaching rate is low, therefore the ion exchange reaction is low. Various strong inorganic acids (HCl, H_2SO_4, HNO_3) can be completely ionized and hence produce high concentrations of protons or hydronium which interact with the surface of the glass [88][91]. These acids can efficiently conduct the ion exchange process at high rate making leaching possible. Borosilicate glasses present lower mass loss compared to soda-lime glasses due to the presence of silicate and borate structural units [88][92]. Depending on the acid used, different salts can be formed: NaCl, $NaNO_3$, $NaSO_4$, hydrolyzing the boric oxide to H_3BO_2 [93].

The reaction mechanisms depend on the composition of the glass and the leaching parameters (temperature, pH and time) [94]. In borosilicate glass, sodium cations are connected to the $[BO_4]^-$ borate groups (in reedmergerite-like and danburite-like structures) to neutralize the charge [95]. Since borate is more soluble than silica in acid solutions and given its connectivity with sodium, during leaching borate and sodium will be extracted together [88].

Kreisberg et al. investigated micro and mesoporosity in a $0.3Al_2O_3$-$6.8Na_2O$-$20.9B_2O_3$-$72SiO_2$ porous glass prepared by leaching in 1 M and 3 M HCl at 100 °C for 9 hours. The chemical composition showed a silica rich porous structure of 96-98 mol% SiO_2, 2- 4 mol% B_2O_3 and traces of alkali. Increasing the concentration of HCl led to a decrease of the total specific surface area of the pores, an increase in pore size of secondary silica clusters, and an increase of the mesopore diameter [96]. Later in a new study, a 93.7 mol% SiO_2, 5.8 mol% B_2O_3, 0.4 mol% Na_2O, 0.1 mol% Al_2O_3 porous glass composition was reported [97].

A leaching study with 1.5 M HCl with different inorganics salts (NaCl, KCl, NH_4Cl, $BaCl_2$) at 98 °C was carried out. Results showed a linear increase in thickness of the leached layer with leaching time [92]. After acid leaching, an alkaline attack performed with 0.5 M KOH at RT for 3 to 6 hours was studied resulting in the removal of the silica cluster from the pores given by the monomodal pore size distribution [84].

Toquer et al. extensively studied the effect of the HCl concentration and leaching time on the pore structure of a $5Na_2O$-$20B_2O_3$-$75SiO_2$ glass. Acid concentrations ranging from 0.1 to 3 M HCl with times of 2-48 h at 90 °C and an acid/glass ration of 10 ml/g were applied.

At 0.1 M HCl, low values of specific surface area and pore volume are reported. As the concentration was increased to 0.7, the latter properties increased as well due to the formation of finely dispersed silica in the pores. Higher HCl concentrations of up to 3 M lower the specific surface area and pore volume. An increase in the colloidal silica diameter is observed under these conditions. Leaching time is another key parameter as it lowers the specific surface area caused by the progressive extraction of silica into the acid solution. Figure 2.15 shows the different morphologies in leached samples as the acid concentration increases [98].

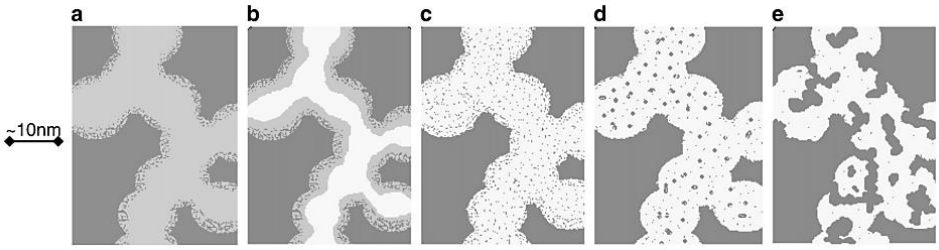

Figure 2.15: Effect of increasing HCl concentrations on the morphology of porous glass. a) phase separated base glass, b) 0.1 M, c) 0.3-0.7 M, d) 1M, e) 3 M [98].

Antropova et al. evaluated how the dissolution of a phase-separated borosilicate glass takes place using HNO_3 and concluded that stirring and the B_2O_3/SiO_2 ratio influence the leaching process [99][100].

Figure 2.16 shows how the leaching process takes place in a phase separated glass (a). At the beginning, a thin leached layer is formed that contains colloidal silica in the pores (b). As leaching progresses inside the glass, a colloidal silica-free layer (with larger pore size) is formed on the surface (c). Below the silica-free layer continues to have residual silica. The process continues with the thickness of the silica-free layer increasing (d-e) until the alkali-borate rich phase is etched [101].

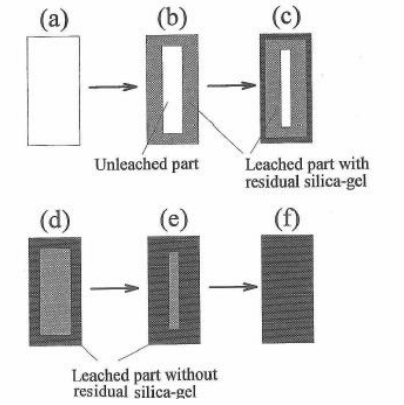

Figure 2.16: Schematic representation of the leaching process [101].

Aboutaleb et al. studied the chemical durability of borosilicate glass before and after annealing in neutral, acidic and alkaline solutions [88]. Mass losses were reported in the case of alkaline solution for non-heat treated glasses.

For neutral and acidic solution no mass loss was identified given the packed structure that avoids any migration inside the network [102].

Adding other elements to the borosilicate composition can bring favorable conditions in phase separation and leaching and improve the chemical stability of the residual glass. Studies determined that adding 8 wt% V_2O_5 and 5 wt% P_2O_5 can improve up to five times the leaching rate [103]. This effect occurs due to a broadening of the immiscibility dome. Lead oxide added to glass produces a structure with smaller pore size and increases the surface area [104]. Opposite results are obtained if Fe_2O_3 is introduced to the glass system, however, it increases the chemical resistance [105]. TiO_2 causes a reduction of the pore size while bigger pores result from the incorporation of Al_2O_3 [106].

Tsyganova [107] reported that using KCl mixed with 3 M HCl induces an increase in the leaching rate as well as the amount of the unstable alkali-borate phase extracted. Adding KCl also promotes the polymerization of secondary silica [108]. Huang, to reduce the probability of sample breaking, used 2 M HCl with NH_4Cl (50/50 proportion) at 115 °C as a leaching solution [109].

Similar leaching conditions were used by Takamori et al., glass probes were immersed in 3 M HCl solution saturated with NH_4Cl at 113 °C for 6 hours. Results showed that for low heat treatment temperatures (550 °C), the leaching rate decreases fast. For 650 °C, there is only a minor increase in the leaching rate (see Figure 2.17) [110].

Flourine additions to the glass composition are reported to also enlarge the pores. It is stated that increasing the acid/glass ratio from 200 ml/g to 500 ml/g, favors the extraction of colloidal silica [101]. A similar study evaluated also the influence of the solution to the glass ratio on leaching. For values above 100 ml/g, the diffusion of the dissolved silica out of the glass is easier, therefore favoring the silica extraction [82].

Takahashi used a ratio of 1 g of glass per 100 ml of HCl to leach an alumino-borosilicate glass. A B_2O_3 extraction of 80 % was achieved at low Al_2O_3 concentrations. Above 4.5 wt% Al_2O_3 the extraction of the soluble phase decreases, as a sign of the reduced degree of phase separation [111].

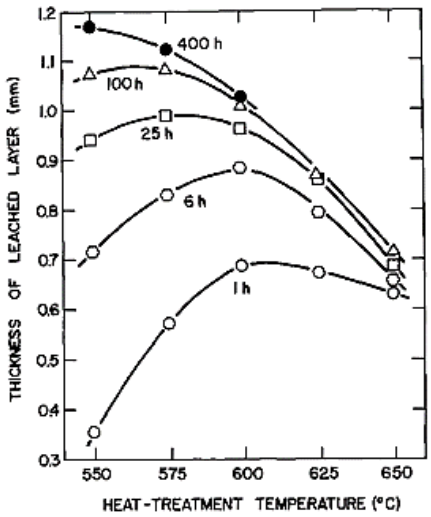

Figure 2.17: Effect of the heat treatment parameter (time and temperature) on HCl leaching [110].

Yazawa et al. added MgO and ZnO to a SiO_2 -B_2O_3-RO-ZrO_2 glass system followed by a heat treatment at 750°C for 10 hours. According to scanning electron microscopy, the phase separation showed a droplet structure for samples with 9.2 mol% MgO or ZnO, thus samples couldn't be leached. It was also noted, that in order to leach ZrO_2 containing glasses, leaching with H_2SO_4 (3 M, at 98 °C for 48 hours) is recommended to extract colloidal ZrO_2 precipitated in the pore walls [64].

Organic acids can also be used for leaching, as was suggested by Eguchi, for instance oxalic acid, acetic acid, succinic acid, and citric acid in 0.2 to 5 N concentrations. In this study, the addition of an alkali earth oxide or ZnO to the glass composition was proposed in order to avoid the transfer of ZrO_2 to the soluble phase during the heat treatment and its removal during leaching, which would result in a poor alkali resistance porous glass. An amount of no less than 5 wt% ZnO is desirable [112].

Rakhimova studied a 16.8Na_2O-39.0B_2O_3-44.0 SiO_2 glass leached at low temperature with a ratio of 50 ml for 1 g of glass. Even at mild leaching conditions, leaching occurs and silica gel from the soluble phase can be found in the solution. After leaching, results showed that 20-30 % SiO_2, 80 % Na_2O and 100 % B_2O_3 were extracted [113]. Lyubavin et al. used similar leaching conditions to fabricate porous membranes, in a 7Na_2O-23B_2O_3-70SiO_2 glass composition heat treated from 570 to 700 °C. Pore diameters up to 110 nm were registered [114].

Shimbo investigated the influence of temperature on the leaching process. Figure 2.18a and Figure 2.18b show the leaching effect of a 3.2Al_2O_3-6.8Na_2O-27.1B_2O_3-62.9SiO_2 glass leached at different concentrations of HCl at 95 °C and 23 °C, respectively. The

leaching rate is higher with higher concentration of HCl but it deflects to constant value as the acid concentration continues to increase (see Figure 2.19) [92]. In another research on a $5Na_2O$-$20B_2O_3$-$75SiO_2$ glass, a 1 mm per day leaching rate using 3 M HCl or 2.5 M H_2SO_4 at 98 °C was registered [115].

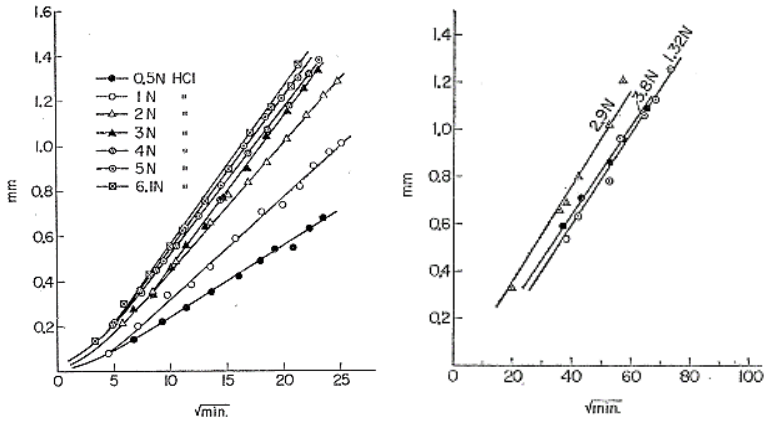

Figure 2.18: Effect of the leaching time at 95 °C (a) and 23 °C (b) on the thickness of the leached layer for a sodium alumino-borosilicate glass [92].

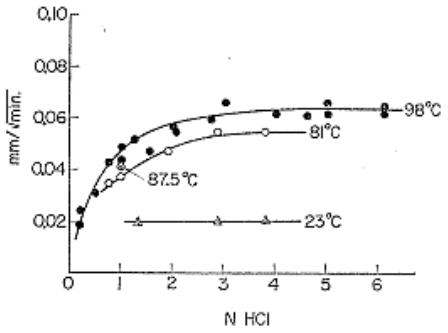

Figure 2.19: Effect of HCl concentration on the leaching rate at different temperatures for a sodium alumino-borosilicate glass [92].

Hammer et al. fabricated porous glass fibers from an initial glass composition of $77SiO_2$-$18B_2O_3$-$5Na_2O$. For heat treatment, temperatures between 450 °C and 750 °C were suggested to successfully phase separate the glass samples. Depending on the fiber matting method different mass losses were obtained (Table 2.2) [116].

Glass fibers after leaching consist of $0.2Na_2O$-$3B_2O_3$-$96.8SiO_2$ [116].

Table 2.2: Weight loss of the phase separated glass reported after leaching in 3 M HCl [116].

		Heat treatment		Leaching (3 M HCl)		
Sample	Preparation	Time (h)	Temperature (°C)	Time (min)	Temperature (°C)	Weight loss (%)
1	H_2O matted	4	580	5	98	22.4
2	H_2O matted	4	580	10	94	24.1
3	H_2O matted	4	580	20	95	25.8
4	H_2O matted	4	580	34	98	27.0
5	No H_2O matted	24	580	10	98	24.5

2.13. Crack formation in porous glasses

As leaching progresses, strain develops inside the glass. A swelling effect on the leached layer creates tensile stress in the adjacent unleached layer. On the contrary, if the leached layer shrinks it undergoes tensile stress. Fracture can occur when stress levels are high. Proper glass compositions and heat treatments can reduce the possibility of cracking [93].

According to Huang, cracking occurs at the end of the leaching process or when the leaching temperature is around 50-70 °C. It was observed that the samples usually split to parallel pieces (see Figure 2.20) due to high tensile stress. Stresses can be generated by a change in volume from a bulk to a porous glass state or by the different thermal expansion coefficients of the phases [109]. These stresses can hardly be released during the heat treatment [117].

Capillary forces cause stress at the interface glass/solution. Given the direct relation between the capillary forces and the surface tension of the acid solution, a surfactant agent such as NaCl, KCl or NH_4Cl can be added to the acid solution to reduce the surface tension. Another method to reduce the surface tension is the elevation of the leaching temperature [104][109][110].

Moreover, considering the surface energy of the glass, during leaching the interface glass/glass is replaced by a glass/acid one. This increases the surface energy of the leached layer causing a contraction as a result of lowering the surface energy [118].

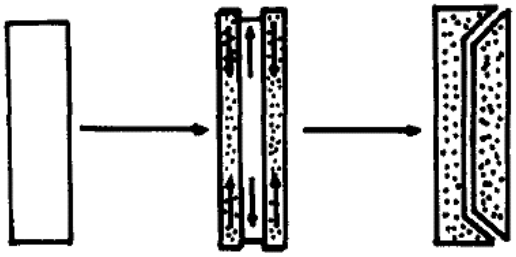

Figure 2.20: Stress formation due to tensile stress in leached and non-leached layers during leaching [109].

Similarly, Scherer et al. evaluated the reasons of stress in glass during leaching and concluded the following [119]:

- Thermal stress: A mismatch in thermal expansion coefficient of the phases causes tension in the phase with higher thermal expansion (borate phase) during cooling. This tension is released during leaching.
- Capillary stress: After the extraction of the soluble phase, a transition of a low to a high energy interface causes a contraction of the porous structure and stress on the leached walls.
- Ion exchange: During leaching, a change in composition occurs in the surface of the pore walls. Protons from the solution can exchange with alkali ions creating a contraction in the glass.
- Hydration: During the ion exchange process (hydronium diffusion), the surface of the pores becomes hydrophilic and water is absorbed. This causes swelling of the glass.

Kukisaki et al. studied a Na_2O-CaO-MgO-Al_2O_3-B_2O_3-SiO_2 glass with different heat treatments and leaching conditions. During the experiments, cracking of the samples was reported as it is shown in Table 2.3. A relationship between crack formation and the presence of silica gel was established. Large amounts of precipitated silica gel in the pores induce a slower diffusion during leaching up to a degree of blocking the process. This generates stresses and cracking of the porous glass membranes [61].

Table 2.3: Evaluation of glass samples condition after leaching [61]. Yes: cracking observed. No: no cracking observed.

Mean pore diameter (nm)	Leaching temperature (°C)				
	30	45	60	75	90
82	No	No	Yes	Yes	Yes
172	No	No	No	Yes	Yes
725	No	No	No	No	No

2.14. Effect of zirconia on the structure and durability of glass

It is well known that even small additions of zirconia can have a strong effect on glass properties: increase of chemical durability, density and glass transition temperature [120]. Zirconia containing glasses are suitable in fields of chromatography [11], glass fibers in fiber-reinforced concrete [121], nuclear waste encapsulation [122][123], etc.. It is of great interest to understand the glass corrosion mechanism in alkaline environments and the effect of ZrO_2 on glass durability [18][124][125].

In silicate glasses, depending on the compatibility of the oxides added to the glass, they will distribute either in the soluble or the insoluble phase after phase separation. As oxide modifier cations compete with Si^{4+} ion for oxygen, phase separation occurs by depolymerization of the glass network due to the modifier cation preference of a coordination surrounding of non-bridging oxygen atoms [43][64]. At lower amounts of ZrO_2 in silicate glasses, the Zr^{4+} ions are mostly located in ZrO_6 octahedra with four bridging and two non-bridging oxygen atoms, the latter linked to network modifier cations [43]. By charge compensating the network modifying ions, NBO at SiO_4 tetrahedra are removed and additional BO are created [62].

Si-O-Si covalent bonds are formed, thus strengthening the silica network [62]. After phase separation and leaching ZrO_2 remains in the insoluble silica phase [43].

The new covalent bonds increase also the chemical durability against alkaline solutions (NaOH, NaH_2PO_4) even at small additions of ZrO_2. It is believed these solutions react with all the components, not only with modifier alkali ions but also with silica network as can be seen in the following reaction [33][87]:

$$\equiv Si\text{-}O\text{-}Si\equiv + Na^+OH^- \rightarrow \equiv Si\text{-}OH + \equiv SiO^-\ Na^+$$

Hydrolysis to -$Si(OH)_3$ radical groups promotes glass dissolution as:

$$\equiv SiO\text{-}Si(OH)_3 + OH^- \rightarrow \equiv SiO^- + H_4SiO_{4\,(aq)}$$

The effect of ZrO_2 can be explained by its ability to remain stable and not hydrate under any pH condition [34].

Du et al. reported a decrease in pore size with higher amounts of ZrO_2 up to 10 wt% in a $9.4Na_2O$-$25.4B_2O_3$-$65.2SiO_2$ glass (see Figure 2.21). ZrO_2 inhibits the process of phase separation slowing down the diffusion of boron away from silica [126].

Hasanuzzaman et al. reported smaller pore sizes with addition of ZrO_2 and $ZrSiO_4$ from 7 to 15 wt%. The investigated $6Na_2O$–$25B_2O_3$–$69SiO_2$ glass was heat treated at 650 °C for 14-63 hours showing pore diameters ranging from 80 to 139 nm. Regarding the durability, 3 to 4 times better alkali resistance was reached in glasses with ZrO_2 and $ZrSiO_4$ [62]. Identical improvements in alkali stability with similar compositions were obtained by Hasanuzzaman et al. in a different research [127].

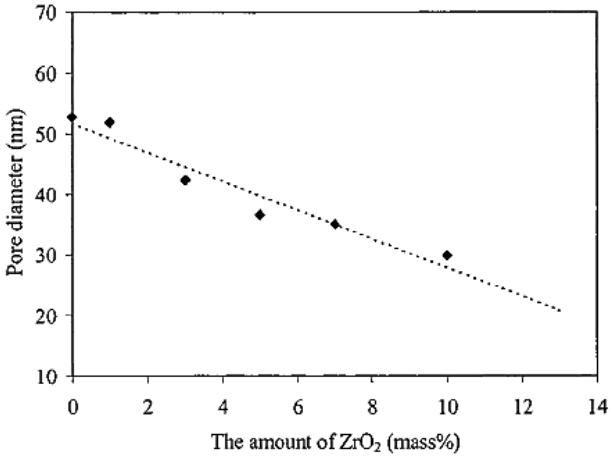

Figure 2.21: Dependence of the pore diameter on the amount of ZrO_2 in a borosilicate glass [126].

The chemical durability of glass depends on glass composition, nature and parameters of the leaching solution. Chemical resistance is usually measured by the mass loss of glass components. De Villiers, in early studies of ZrO_2 in glass, evaluated a Na_2O-B_2O_3-Y_2O_3-ZrO_2 glass with 12 wt% ZrO_2. Though the samples were not completely leached and broke during handling, an alkali resistance of 0.0041 mg/dm^2 was reported [128]. This result shows a great improvement in alkali resistance, if silica is completely substituted by Y_2O_3 and zirconia is added to the glass composition, compared to the 0.35 mg/dm^2 value obtained for a zirconia free glass [62].

Kukizaki et al. investigated the durability effect of ZrO_2 on the crystallization and phase separation in a porous glass of the composition $6.6Na_2O$-$19.6CaO$-$4.8Al_2O_3$-$17.3B_2O_3$-$51.7SiO_2$ with additions of 1-5 mol% of ZrO_2. It was reported that ZrO_2 leads to a slower growth rate of spinodal phase separation. This can be explained by a higher viscosity due to the ZrO_2 addition and the lower mobility of atoms. Alkali leaching tests were carried out with 1 M NaOH at 30 °C for up to 20 hours. Results indicated that the glass composition with 3.5 mol% ZrO_2 exhibits 3.5 times higher alkali resistance than the ZrO_2-free glass [43].

Similarly, Morimoto improved alkali resistance values with additions of ZrO2, SnO2 and Al2O3. For glasses with 5.7 wt% ZrO2, the chemical stability against 0.5 M NaOH was increased up to 4 times in comparison to Vycor® glass [124].

Nakashima et al. investigated the improvement in alkali stability of a $10Na_2O$-$25B_2O_3$-$65SiO_2$ base glass with ZrO_2 (2-8 mol%) and CaO (2-10 mol%) additions. A relationship between the concentration of ZrO_2 in the final porous structure with the presence of CaO was determined. If CaO concentration is higher than 3 wt%, the concentration of ZrO_2 increases in the residual porous glass structure [125].

A direct influence of weight loss with time during alkali leaching (1 M NaOH at 30 °C) was observed (see Figure 2.22). The alkali durability was increased in glass compositions G and H by 8-10 times compared to ZrO_2-CaO free glass [125].

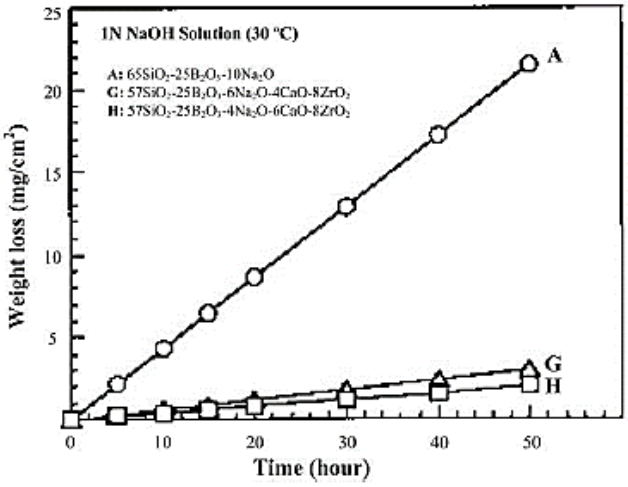

Figure 2.22: Weight loss dependence on leaching time for porous glasses with and without ZrO_2/CaO addition heat treated at 700 °C for 15 hours [125].

Other methods have been used to improve alkali resistance with ZrO_2. Murakami et al. coated a porous glass with a ZrO_2 thin film by immersion in a zirconium alcoholate solution. A reduction from 28.4 to 7.3 wt% loss was registered [129]. A similar procedure was carried out by Tomb et al.. A ZrO_2 barrier on the porous glass surface was produced by a using $ZrCl_2$ solution [130].

CHAPTER 3

3. Experimental procedure

3.1. Glass composition

Glasses with three different compositions were prepared. A base glass (BG) composition of $6.4Na_2O$, $20.7B_2O_3$, $72.9SiO_2$ without ZrO_2 was chosen. Silica was substituted by Zirconia to evaluate the effect on chemical durability against alkali solutions. The compositions were chosen to be within the immiscibility gap (see Figure 3.1) of the Na_2O-B_2O_3-SiO_2 ternary system [33]. Table 3.1 shows the glass compositions (mol%).

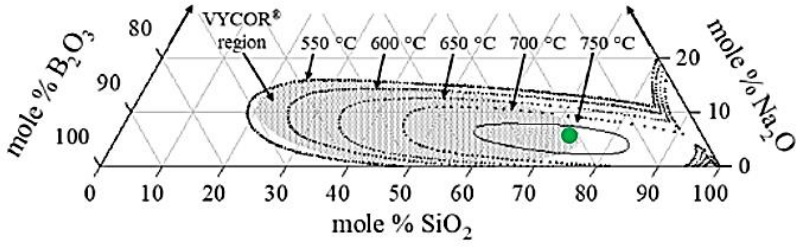

Figure 3.1: Position of the investigated Zr0-BG ($6.4Na_2O$, $20.7B_2O_3$, $72.9SiO_2$) in the ternary system Na_2O-B_2O_3-SiO_2 [69].

Table 3.1: Glass batch compositions. SiO_2 is substituted with two different ZrO_2 concentrations.

Glass name	Glass composition (mol%)			
	SiO_2	B_2O_3	Na_2O	ZrO_2
Zr0-BG	72.9	20.7	6.4	-
Zr3-BG	69.9	20.7	6.4	3
Zr6-BG	66.9	20.7	6.4	6

3.2. Glass synthesis

SiO_2, B_2O_3, $NaCO_3$, NaCl, $NaNO_3$ and $ZrSiO_4$ were used to fabricate base glasses with a conventional melting process. Batches of 200 g per glass composition were prepared by mixing the raw materials. To compensate the evaporation loses of B_2O_3 during melting, additional 10 wt% of B_2O_3 was added to the batch. NaCl and $NaNO_3$ (1.35 wt% and 1.96 wt%, respectively), as part of the 200 g batch, were used to reduce the melt viscosity and as refining agents to remove bubbles from the melt. A Pt crucible with the batch was placed in an air atmosphere furnace pre-heated at 1450 °C (Nabertherm HFL 16/17).

Every 15 min, the crucible was taken out and moved around to homogenize the melt and to eliminate bubbles. After 1.5 hours, the temperature was gradually increased to 1550 °C and kept constant for 0.5 hours to lower the viscosity and favor an adequate casting. For Zr3-BG and Zr6-BG, the casting temperature had to be raised up to 1600 °C.

After casting, samples were annealed in a 540 °C pre-heated furnace (Nabertherm LH 30/13) for 6 hours and subsequently the furnace was switched off and cooled down to room temperature. The obtained glass samples were transparent with no signs of cracking. The melting and annealing processes are shown in Figure 3.2.

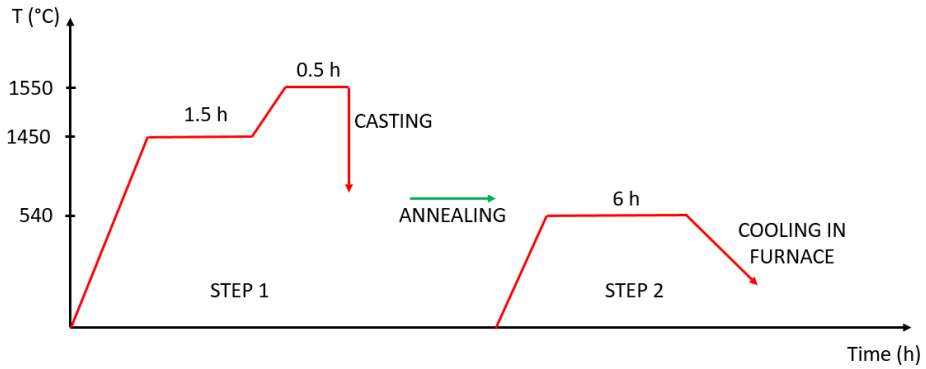

Figure 3.2: Melting and annealing processes.

3.3. Heat treatment process and phase separation at different temperatures

After casting, samples were cut and polished with resin-bonded diamond grinding disc grits #80, #120, #220, #600 and SiC grinding paper grit #800, #1200, #2500, #4000 (final sample thickness 1.5-1.7 mm) in order to obtain smooth surfaces and to better visualize the phase separation effect.

The range of temperature at which phase separation occurs depends on the glass composition. At higher temperatures than the upper limit (critical temperature), phase separation does not take place. If the temperature is too low, the high viscosity prevents the phase separation. In this research, to evaluate the phase separation phenomena, glass samples of all compositions were heat treated at different temperatures for 12 hours and leached in 1 M HCl for 1 hour (see Table 3.2).

Table 3.2: Summary of all heat treated glasses.

Glass Name	Heat treatment temperature (°C)	Glass Name	Heat treatment temperature (°C)
Zr0-560	560	**Zr3-600**	600
Zr0-580	580	**Zr3-620**	620
Zr0-600	600	**Zr3-640**	640
Zr0-620	620	**Zr3-660**	660
Zr0-640	640	**Zr3-680**	680
Zr0-660	660	**Zr3-700**	700
Zr0-680	680	**Zr6-600**	600
Zr0-700	700	**Zr6-620**	620
Zr3-560	560	**Zr6-640**	640
Zr3-580	580	**Zr6-660**	660

3.4. Glass characterization

3.4.1. Density by gas pycnometer

The pycnometer AccuPyc 1330 (Micromeritics) was used to determine the volume of the glasses. This is a non-destructive technique that measures volume and calculates the density of solid samples using the gas displacement method. Helium is usually used due to its small atomic size that allows entering the pores. The volume measured is the total space which the gas cannot enter. The sample is introduced in a chamber of known volume (V_c). Helium is added to the system and expanded into another chamber of volume V_r. The pressure before (P_1) and after expansion (P_2) are registered to measure the sample volume (V_s) (see Figure 3.3.). Assuming ideal gas behavior and fast expansion equilibrium, the sample volume and density are calculated according the following Eq. 8 and Eq. 9 [131][132]:

$$V_s = V_c + (V_r/(1-P_1/P_2)) \qquad \text{(Eq. 8)}$$

$$\rho = ms/Vs \qquad \text{(Eq. 9)}$$

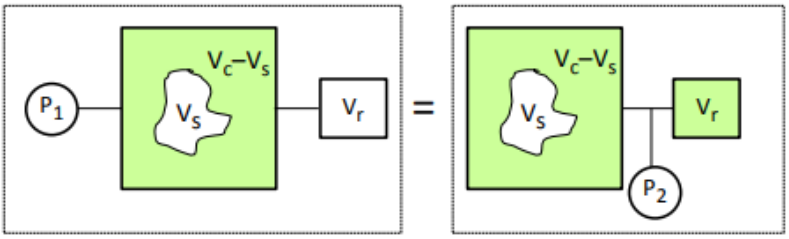

Figure 3.3: Gas pycnometer principle. Before expansion (left), after expansion (right) [132].

3.4.2. Differential scanning calorimetry

Differential scanning calorimetry (DSC) is a technique that identifies thermodynamic events such as glass transition temperature T_g, a 2nd-order phase transition. Heat flow is measured as temperature in the sample chamber is increased or lowered and chemical and/or physical reactions occur in the sample, which are related to a release (exothermic) or consumption (endothermic) of energy. The measurements were carried out under air atmosphere at a heating rate of 10 K/min in a Pt-Rh crucible from 100 °C to 1300°C. The equipment used was a Netzsch STA 409 PC.

There are three ways to determine the T_g with a DSC (see Figure 3.4). The “onset method”, which requires to draw two tangent lines. The first tangent at the beginning of the transition, the second tangent along the first slope. The “inflection point method” is calculated mathematically. The “peak method” uses tangent lines at the end of the transition [133][134]. In this work the onset method was used.

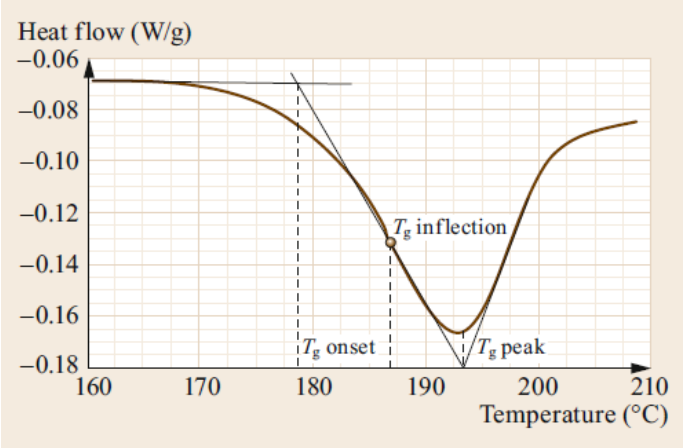

Figure 3.4: Methods to determine the glass transition temperature [134].

3.4.3. X-ray diffraction

X-ray diffraction is a non-destructive technique used to evaluate the nature of crystalline or amorphous materials. A monochromatic X-ray interacts with the sample in a range of angles. Base glasses were analyzed with a Bruker D5000 diffractometer using cobalt radiation (40 kV, 35 mA, 1.78 Å) between angles 10-90° (2θ). The crystalline phase present in the glass was detected using the Match 3.12 software (Crystal Impact). A scheme of a diffractometer is shown in Figure 3.5.

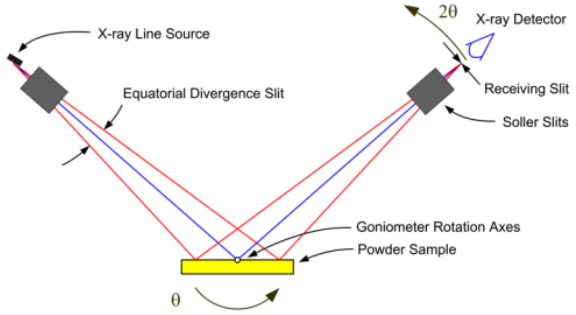

Figure 3.5: Schematic representation of a diffractometer [135].

3.4.4. Scanning electron microscopy (SEM)

Scanning electron microscopy is one of the most versatile techniques to examine and analyze the surface of materials (features, texture, shape and size of particles on the surface). High magnifications can be achieved due to a high energy electron beam use which irradiates the sample and induce emission of secondary and backscattered electrons. The electrons will be registered by the detector. The secondary electrons are the valence electrons which have low energy, therefore only the ones near the surface can be emitted outside the sample. They give information of the surface with good resolution. Backscattered electrons have higher energy than secondary electrons, thus they provide information (compositional and topographic) from deeper in the sample. The higher atomic number the brighter a zone will appear in the image as more secondary electron will be detected. When an electron is unable to reach the detector a dark region is generated [136][137]. A schematic representation can be observed in fig. 3.6. Glass phase separation was examined with a Hitachi S-4800 scanning electron microscope and a Thermo Fisher Scientific SDD NORAN7 detector.

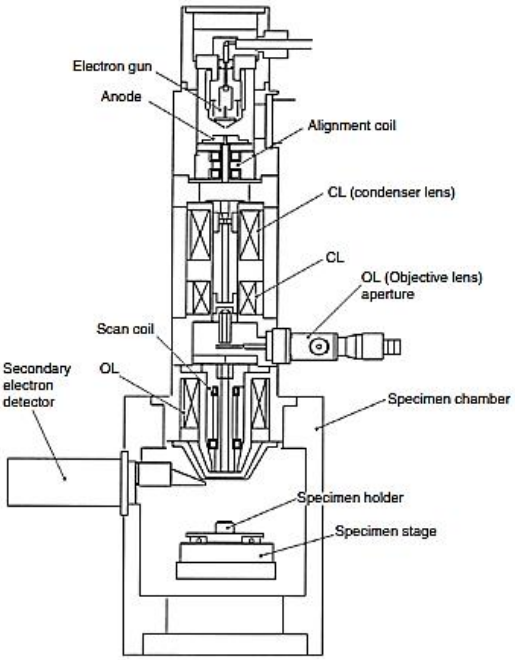

Figure 3.6: Schematic diagram of a scanning electron microscope [137].

3.4.5. Attenuated total reflectance (ATR)

ATR is a technique used in infrared spectroscopy. A crystal with higher refractive index is in contact with the sample. Through total internal reflection, an IR beam produces an evanescent field in the sample which can penetrate 0.5 to 2 µm (see Figure 3.7). The absorption of this wave is used to graph the IR spectrum. Measurements were carried out in a Thermo Fisher Scientific Nicolet™ iS™ 5 FTIR Spectrometer using a diamond crystal.

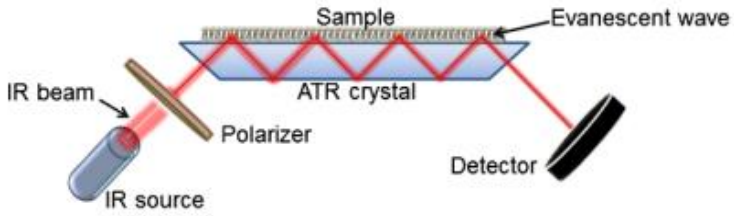

Figure 3.7: Schematic representation of the ATR working principle [138].

3.4.6. Pore size analysis

After phase separation and leaching for 1 h at room temperature in 1 M HCl, scanning electron microscopy images were prepared to confirm phase separation. According to DIN EN ISO 13383 [139], lines were drawn diagonally and the software ImageJ was used, according to scale, to measure the size of grains or in this case of pores after extraction of the soluble phase as can be seen in Figure 3.8. Depending on the pore size of the SEM images, a minimum of 20 pores was measured per image.

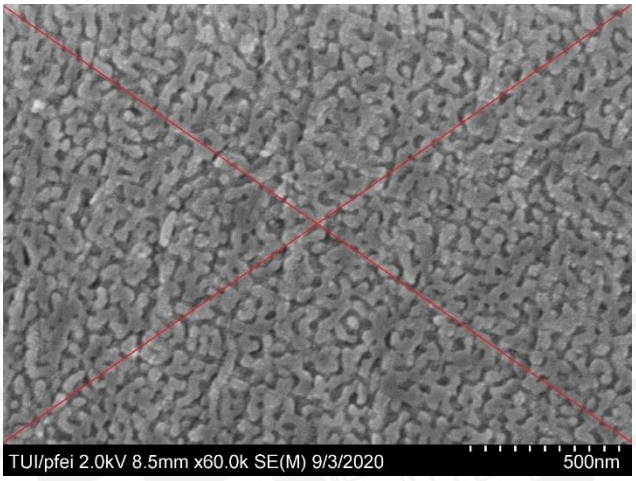

Figure 3.8: Measuring method according the DIN EN ISO 13383 norm.

3.5. Porous glass fabrication

The leaching tests that were previously carried out to determine the pore sizes and confirmed the extraction of the soluble phase. However, under those conditions it is difficult to confirm if the extraction was not only on the surface but also throughout the thickness of the sample. The biggest difference in pore size results between Zr0 and Zr3 glasses were observed at a phase separation temperature of 680 °C. To compare the mechanical strength of the porous glasses, 680 °C was chosen to phase separate new samples. Leaching on Zr6 glasses was not performed due to an incomplete phase separation of the samples.

Samples were leached using different parameters to obtain fully leached samples. As leaching time increases, a mass loss is registered. In theory, once the mass loss remains constant, no more alkali-borate phase is left to be extracted. The tests are classified in 3 stages according to the heat treatment of the samples and the leaching solution:

3.5.1. Acid leaching - stage 1

Samples were phase separated at 680°C for 12 hours and leached in 1 M HCl, with an acid/glass ratio of 100 ml/g (see Table 3.3). After acid leaching, the samples were washed:

- 45 min in distilled water,
- 10 min in distilled water using ultrasonic bath.

Afterwards the samples were dried in air at room temperature (RT ≈ 25 °C) or at 90 °C in an oven.

Table 3.3: Acid leaching parameters in stage 1.

Sample	Acid leaching conditions			Drying step (°C)
	HCl (M)	Time (hours)	Temperature (°C)	
Zr3-680	1	16	25	25
Zr3-680	1	24	25	90
Zr3-680	1	26	60	25
		Time (days)		
Zr3-680	1	2	85	25
Zr3-680	1	5	60	25
Zr0-680	1	1	60	25
Zr0-680	1	3	25	25

3.5.2. Acid leaching - stage 2

To reduce the surface tension in the samples during leaching, a new leaching solution was used. The 1 M HCl solution was mixed with 70% Ethanol (surfactant) at a ratio of 9 to 1. After phase separation at 680 °C for 12 hours the samples were leached using the new solution with an acid/glass ratio of 50 ml/g for different periods of time and different temperatures (see Table 3.4). After leaching, samples were washed:

- 20 min in distilled water + 70 % ethanol at a ratio of 1:1,
- 20 min in 70 % ethanol followed by 10 min using ultrasonic bath.

Afterwards the samples were dried in air at room temperature for 24 hours.

Table 3.4: Acid leaching parameters in stage 2.

Sample	Acid leaching conditions			Drying step (°C)
	HCl (M)	Time (days)	Temperature (°C)	
Zr3-680	1	5	70	25
Zr3-680	1	13	70	25
Zr0-680	1	2	25	25

3.5.3. Acid leaching - stage 3

Samples were phase separated at 680 °C and subsequently kept at 560°C for 6 hours to remove residual stress and leached and washed as described in stage 2 (see Table 3.5). Afterwards the samples were dried in air at room temperature for 24 hours.

Table 3.5: Acid leaching parameters in stage 3

Sample	Acid leaching conditions			Drying step (°C)
	HCl (M)	Time (days)	Temperature (°C)	
Zr3-680	2	15	70	25
Zr0-680	2	4	25	25

3.6. Alkali resistance

Alkali stability is important in separation processes because NaOH is used for fouling cleaning of porous membranes. The alkali resistance against NaOH was measured according to the parameters presented in Table 3.6. After acid leaching and drying and samples were immersed into 0.1 M NaOH for up to 22 hours. Weight loss was calculated according to the following equation (Eq. 10):

$$Weight\ loss\ (\%) = \frac{\mathrm{M1\ (g)} - \mathrm{M2(g)}}{M1} \times 100 \qquad \text{(Eq. 10)}$$

Where:

M1: mass before alkali attack

M2: mass after alkali attack

Table 3.6: Alkali resistance measurement parameters.

Sample	Acid leaching conditions			Drying step (°C)	Alkali leaching conditions			Drying step (°C)
	Solution	Time (days)	Temperature (°C)		NaOH (M)	Time (hours)	Temperature (°C)	
Zr0-660	1 M HCl	1	25	25	0.1	22	25	25
Zr3-660	1 M HCl	1	25	25	0.1	22	25	25
Zr0-680	2 M HCl + Ethanol	2	25	25	0.1	22	25	25
Zr3-680	1 M HCl + Ethanol	7	70	25	0.1	22	25	25

CHAPTER 4

4. Results and Discussion

4.1. Visual aspect of phase separated glasses

Glasses in this research showed a good transparency after melting and casting. However, as heat treatment was applied at different temperatures, different degrees of opacity became noticeable. Phase separated glasses, which previously have been cut and polished to a thickness of 1.5 to 1.7 mm, are characterized by increasing opacity if the phase separated pores increase in size. Opacity occurs due to the interaction of light with structural features (separated phases) which have different refractive index values. Light scattering is influenced by the size and number of the particles suspended or dispersed.

Figure 4.1 shows the Zr0-BG samples and Zr0 samples after heat treatments at 580, 620, 640, 660, and 680 °C for 12 hours. In the case of Zr0-BG and Zr0-580, there are no signs of opacity but as the temperature increases samples become opaque and white at 680 °C.

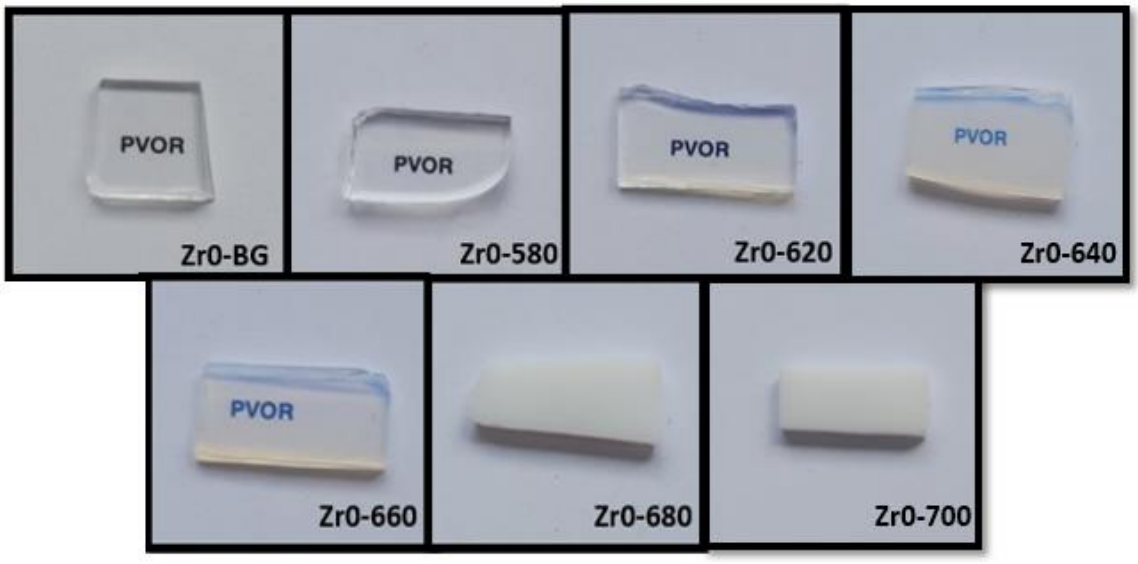

Figure 4.1: 0 mol% ZrO_2 glasses before and after heat treatment at different temperatures for 12 hours. The samples are around 1-2 cm long.

In Figure 4.2 the Zr3 samples are shown before and after the same heat treatment conditions. At 580 °C no opacity is observed. As the temperature increases at 620, 660 and 680 °C opacity increases as well. In contrast to Zr0-680, Zr3-680 still presents a degree of transparency (not fully white). Additionally, samples were treated at 660 °C to evaluate the time dependent phase separation (see Figure 4.3). It was observed that even at low times of heat treatment, phase separation occurs and it progresses with time (higher opacity).

Figure 4.2: 3 mol% ZrO_2 glasses before and after heat treatment at different temperatures for 12 hours. The samples are around 1-2 cm long.

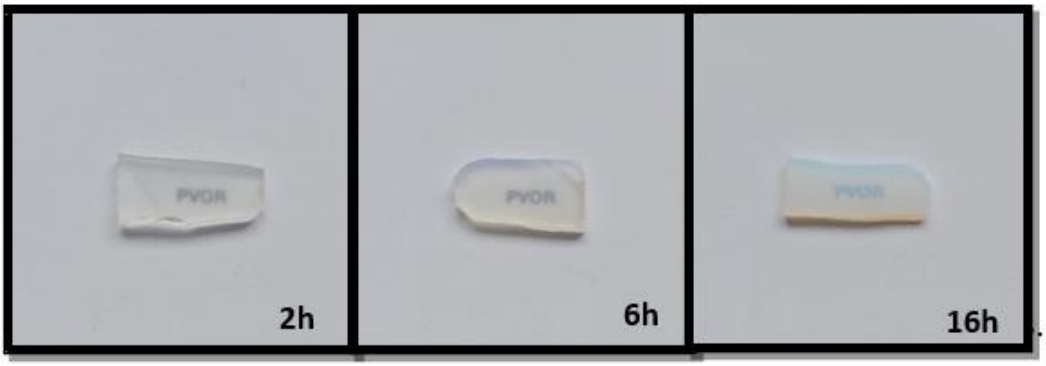

Figure 4.3: 3 mol% ZrO_2 glasses heat treated at 660 °C for different times. The samples are around 1-2 cm long.

In Figure 4.4 glasses with 6 mol% of zirconia were heat treated until 660 °C. Glasses up to 620 °C did not show any opacity. At higher temperatures opacity is observed but it is not uniformly distributed in the sample. This result doesn't follow the tendency of inhibition and the slowing down effect of phase separation, compared to samples with 0 and 3 mol% ZrO_2, as the zirconia content is higher (less opacity at same temperature) due to a possible effect of zirconia crystallization shown in following XRD results.

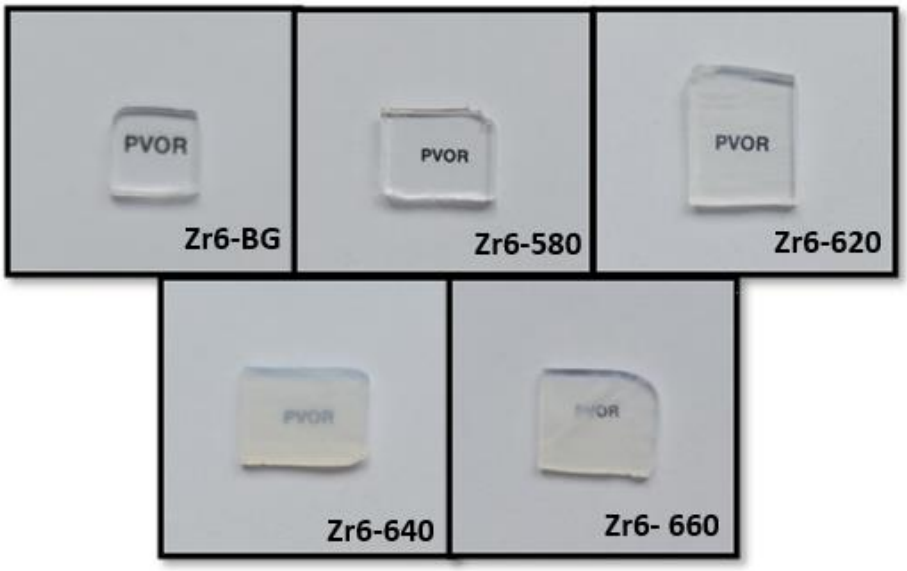

Figure 4.4: 6 mol% ZrO_2 glasses before and after heat treatment at different temperatures for 12 hours. The samples are around 1-2 cm long.

4.2. Density

Density values measured using a pycnometer are shown in Figure 3.5. Values of 2.27, 2.30 and 2.37 g/cm^3 were obtained for Zr0-BG, Zr3-BG and Zr6-BG respectively. The density increases with higher content of zirconia. Since, the glass compositions were made by replacing SiO_2 for ZrO_2, the higher density of zirconia (5.68 g/cm^3) compared to silica (2.65 g/cm^3) does increase the density of the base glasses.

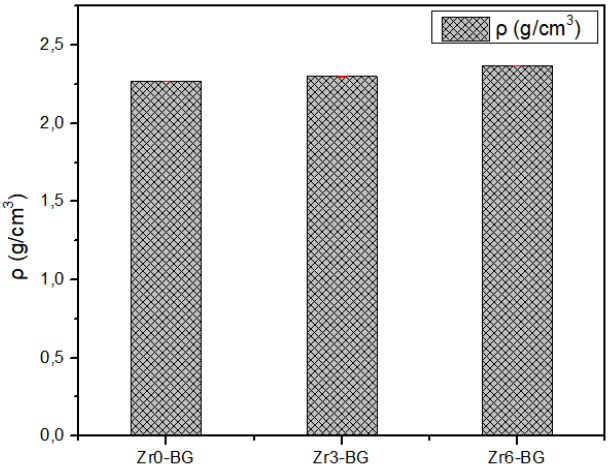

Figure 4.5: Density variation in Zr0-BG, Zr3-BG and Zr6-BG glasses.

Density analysis of porous glass were also carried out on 0 mol% ZrO_2 and 3 mol% ZrO_2 glasses leached under stage conditions 3 and 2, respectively (see Figure 4.6). For the 3 mol% ZrO_2 sample, a decrease in density is observed with longer periods of leaching. After 9 days, a density of 2.14 g/cm^3 was obtained. For 0 mol% ZrO_2 an unexpected increase in density occurs. Further investigation is required to understand this result.

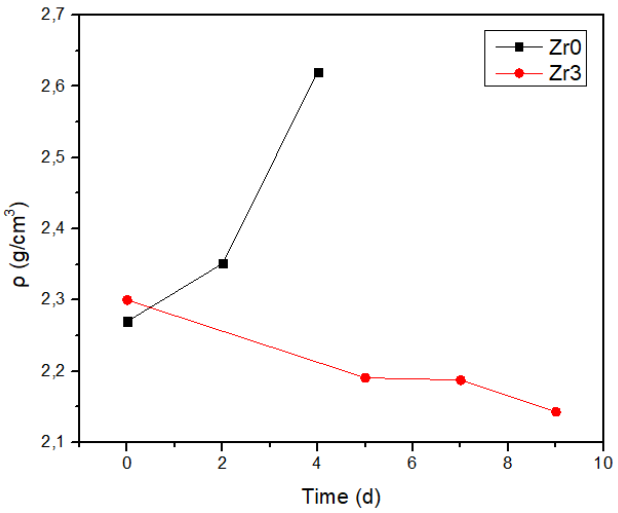

Figure 4.6: Effect of leaching time on the density of 0 and 3 mol% glasses.

4.3. Differential scanning calorimetry (DSC)

DSC analyses were carried out to determine the influence of ZrO_2 on the glass transition temperature (T_g), following the onset method. Zr0-BG and Zr3-BG exhibit similar T_g around 505 °C (see Figure 4.7), however, for Zr6-BG, the glass transition temperature increases up to 520 °C (see Figure 4.8).

As ZrO_2 content increases, Si-O-Si covalent bonds are formed and the number of bridging oxygens per silicon increases, thus strengthening the glass network and increasing the glass transition temperature [62]. Crystallization (exothermic) peaks are present between 550 and 900 °C for all compositions, but it is most pronounced for the Zr6-BG at 850 °C. In fact, ZrO_2 is often used as a nucleating agent for glass ceramics promoting crystallization of glasses.

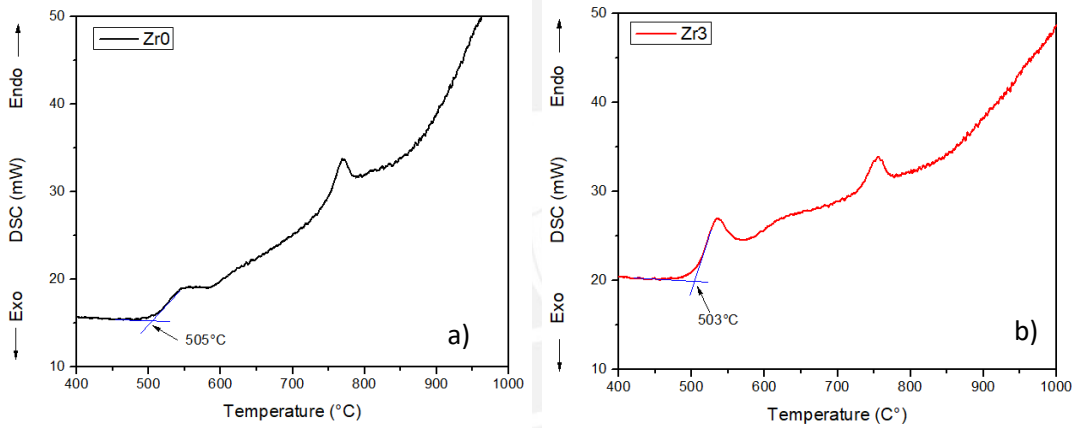

Figure 4.7: DSC curves for glasses with a) 0 mol% ZrO_2 and b) 3 mol% ZrO_2

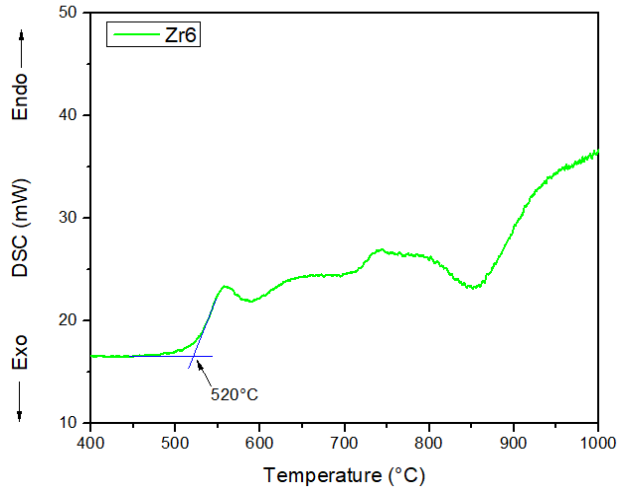

Figure 4.8: DSC curve for glass with 6 mol% ZrO_2

4.4. X-ray diffraction (XRD)

X-ray diffraction was used to identify if any crystallization is present in the samples. Results for Zr0-BG, Zr3-BG and Zr6-BG (see Figure 4.9) show a characteristic diffraction hump between 15 - 35° (2θ). It indicates the amorphous state. No specific diffraction peaks are observed in theses glasses.

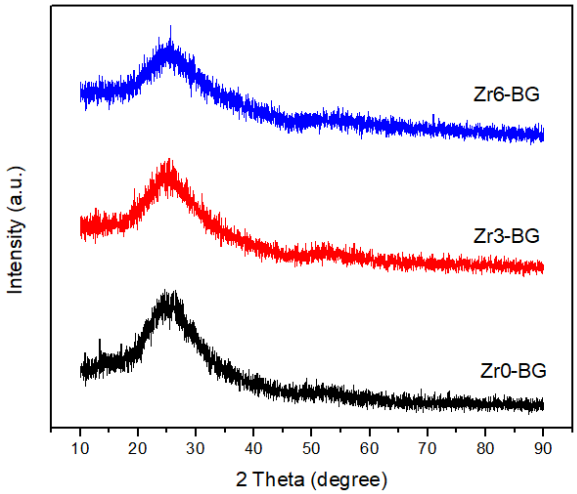

Figure 4.9: XRD pattern for Zr0-BG, Zr3-BG and Zr6-BG. No specific diffraction peaks are observed.

In the case of Zr6-640 glass (see Figure 4.10), the pattern shows a similar hump between 15-35° (2θ). However, different peaks are visible at 35°, 41°, 59° and 71° (2θ). These diffraction peaks were identified as arkelite phase (ZrO_2, ICSD PDF Nr. 01-081-1550).

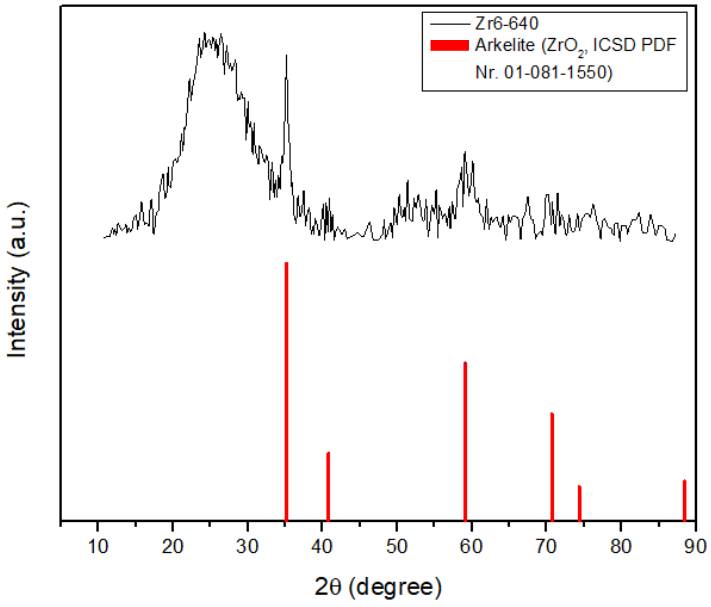

Figure 4.10: XRD pattern for Zr6-640 and the reference pattern for arkelite (ZrO_2).

4.5. Attenuated total reflectance (ATR)

In the infrared spectra, the absorption peaks of mainly silicate and borate groups are to be found along with their different vibrational modes. In the range of 1200-1600 cm^{-1} B-O asymmetric stretching modes of trigonal $[BO_3]$ groups are present [139][140]. B-O stretching modes of $[BO_4]^-$ units exhibit a band between 800-1200 cm^{-1} [91]. Peaks around 700 cm^{-1} can be attributed to B-O-B bending modes [141][142]. Overlapping occurs since silicate groups are also present in the glasses. Symmetrical stretching and bending vibrations of Si-O-Si bonds occur between 755 and 800 cm^{-1} and at around 680 cm^{-1}, respectively. Asymmetrical stretching and bending vibrations of Si-O-Si bonds are observed between 1120-1175 cm^{-1} and at around 470 cm^{-1}, respectively [91]. Stretching vibration modes of Si-O bonds occur between 955 and 970 cm^{-1} [144][145]. Also at 470 cm^{-1}, Zr-O vibrations were reported by Singh et al. [146]. Table 4.1 and 4.2 indicate the groups and vibration modes found in the analyzed glasses.

Table 4.1: Energy of the registered IR absorption bands between 450-900 cm^{-1}.

	Peak band 1		Peak band 2		Peak band 3	
Glass	Energy (cm^{-1})	Designation	Energy (cm^{-1})	Designation	Energy (cm^{-1})	Designation
Zr0-BG	660-680	B-O-B bending mode + Si-O-Si symmetrical bending mode	770-790	B-O stretching mode in $[BO_4]^-$ + Si-O-Si symmetrical stretching mode	870-890	B-O stretching mode in $[BO_4]^-$
Zr0-600	660-680		770-790		870-890	
Zr0-680	660-680		770-790		870-890	
Zr3-BG	660-680		770-790		870-890	
Zr3-600	660-680		770-790		870-890	
Zr3-680	660-680		770-790		870-890	
Zr6-BG	660-680		770-790		870-890	
Zr6-560	660-680		770-790		870-890	
Zr6-600	660-680		770-790		870-890	

Table 4.2: Energy of the registered IR absorption bands between 900-1400 cm^{-1}.

	Peak band 4		Peak band 5		Peak band 6	
Glass	Energy (cm^{-1})	Designation	Energy (cm^{-1})	Designation	Energy (cm^{-1})	Designation
Zr0-BG	960-980	B-O stretching modes in $[BO_4]^-$ + Si-O stretching mode	1100-1200	Si-O-Si asymmetrical stretching mode	1360-1380	B-O asymmetric stretching modes in $[BO_3]$
Zr0-600	990-1010		1100-1200		1360-1380	
Zr0-680	990-1010		1100-1200		1360-1380	
Zr3-BG	960-980		1100-1200		1340-1360	
Zr3-600	960-980		1100-1200		1360-1380	
Zr3-680	960-980		1100-1200		1360-1380	
Zr6-BG	960-980		1100-1200		1360-1380	
Zr6-560	960-980		1100-1200		1360-1380	
Zr6-600	960-980		1100-1200		1360-1380	

Figure 4.11 shows the infrared absorption spectra of glasses after heat treatment at 600 °C. No effect of zirconia addition on the IR absorption was found. Figures 4.12, 4.13 and 4.14 show the infrared absorption spectra of glasses with varying concentrations of zirconia after heat treatment at different temperatures. A very similar behavior was found, almost no influence of the temperature on the peaks was registered. Different results are found in literature, where at higher heat treatment temperatures (higher degree of phase separation), the asymmetric Si-O-Si stretching peak energy increases until 680 °C for a borosilicate glass containing 7 wt% of ZrO_2 [127].

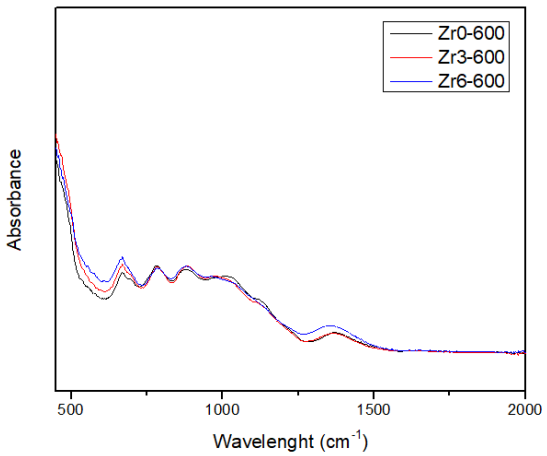

Figure 4.11: Infrared spectra of heat treated glass at 600 °C with 0, 3 and 6 mol% ZrO_2.

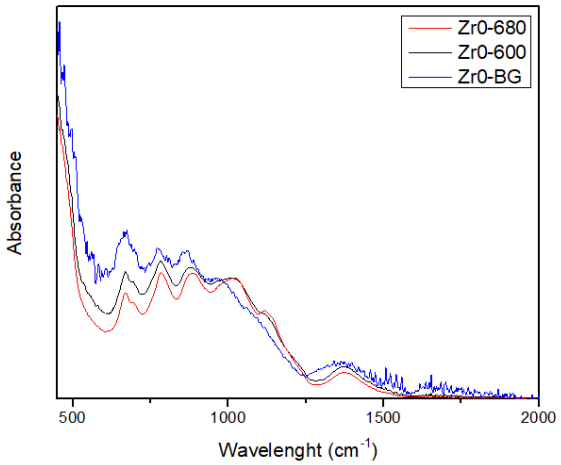

Figure 4.12: Infrared spectra of glass with no ZrO_2 at different heat treatment temperatures.

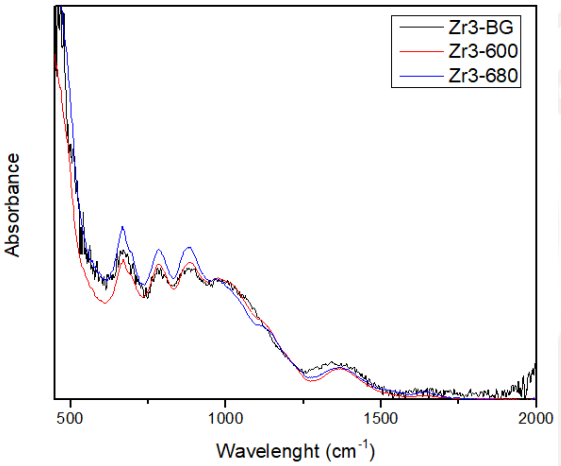

Figure 4.13: Infrared spectra of glass with 3 mol% ZrO_2 at different heat treatment temperatures.

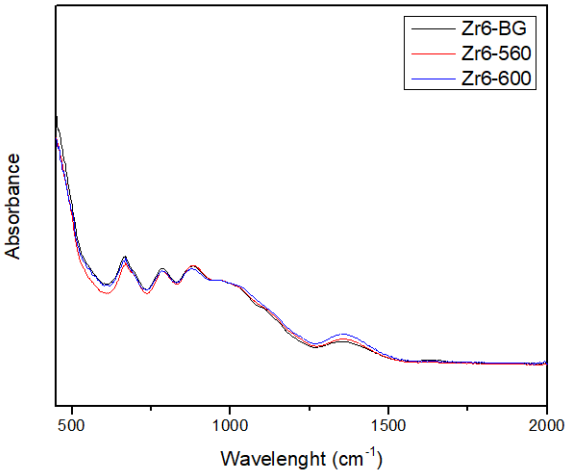

Figure 4.14:Infrared spectra of glass with 6 mol% ZrO_2 at different heat treatment temperatures.

4.6. Scanning electron microscopy (SEM)

To evaluate the morphology of the glasses after heat treatment and leaching (1 M HCl, 1 hour), SEM analyses were carried out. Glasses containing 0 and 3 mol% ZrO_2 (see Figures 4.15 and 4.16) exhibit interconnected phase structures, an indication of spinodal phase separation. At lower temperatures, a low degree of phase separation is observed for the 0 mol% ZrO_2 glass (see Figures 4.15a and 4.15b). At higher temperatures, the borate phase pores are notably bigger, confirming an increasing phase separation tendency as temperature is raised. A similar behavior is observed for glasses containing 3 mol% of ZrO_2 (see Figure 4.16). However, phase separation seems to be inhibited as pore sizes are smaller within the range of heat treatment temperatures (560-700°C).

The morphology of glasses with 6 mol% of ZrO_2 differs from the ones discussed before (see Figure 4.17). Spinodal phase separation does not occur properly in glasses heat treated within 600-660 °C. According to XRD results, the crystalline phase arkelite was detected. Crystalline particles of ZrO_2 were also obtained when 5 mol% ZrO_2 was added to a $Na_2O–CaO–Al_2O_3–B_2O_3–SiO_2$ glass system in an attempt to prevent the crystallization of wollastonite ($CaSiO_3$) [43].

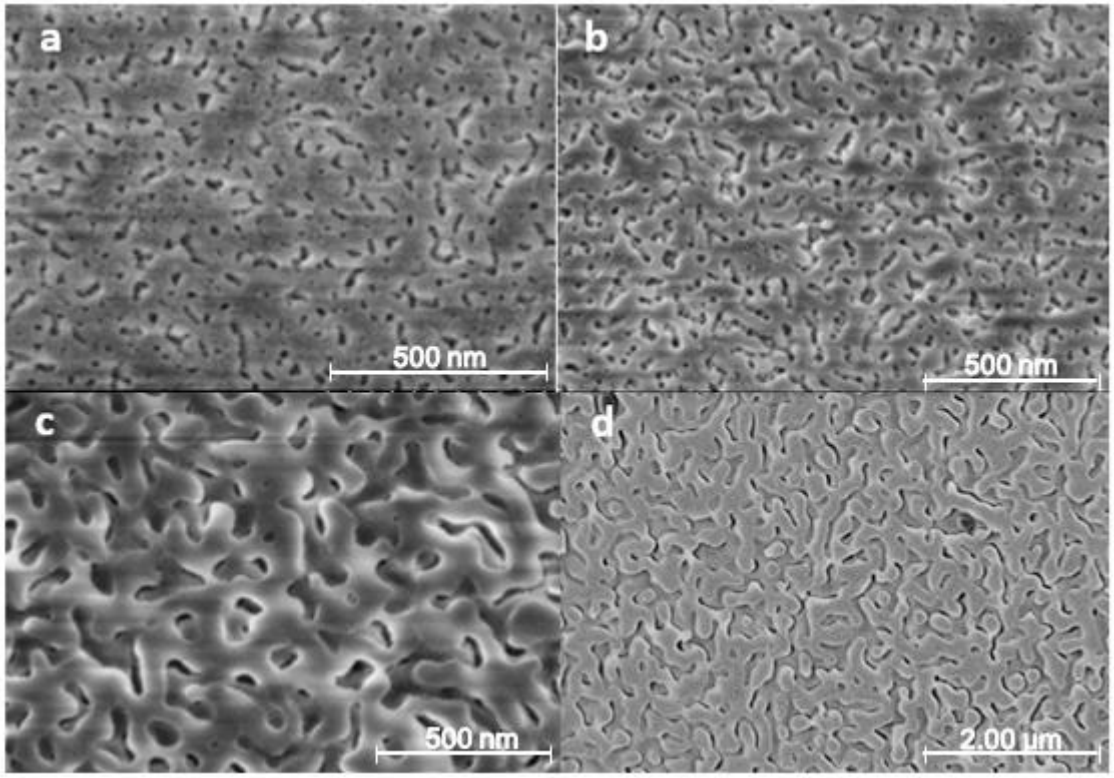

Figure 4.15: Morphologies of heat treated (12 hours) and leached glasses:
a) Zr0-560 °C, b) Zr0-580 °C, c) Zr0-660 °C and d) Zr0-700 °C.

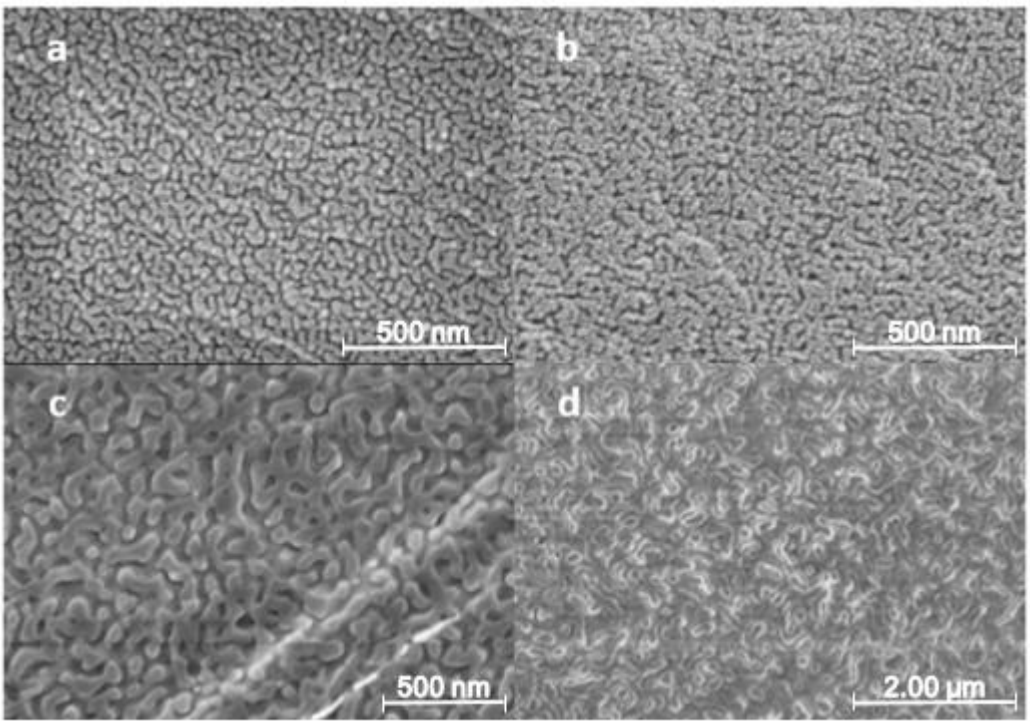

Figure 4.16: Morphologies of heat treated (12 hours) and leached glasses: a) Zr3-560 °C, b) Zr3-580 °C, c) Zr3-660 °C and d) Zr3-700 °C.

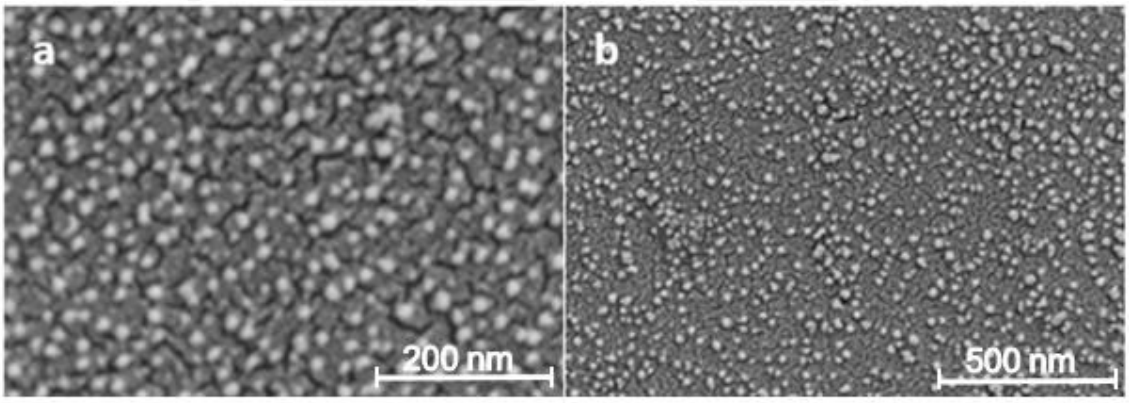

Figure 4.17: Morphologies of heat treated (12 hours) and leached glasses: a) Zr6-600 °C, b) Zr3-660 °C

4.7. Pore size analysis

Pore sizes were calculated according the DIN EN ISO 13383 norm. According to Figure 4.18, a clear tendency can be observed. There is an increase in pore size in both glass compositions if the heat treatment temperature is raised. This is due to a decrease in viscosity that improves phase separation as the diffusion of the borate away from the silica rich phase takes place [77].

For Zr0-700 and Zr3-700 glasses, pore sizes up to 120 and 100 nm were achieved, respectively. Additionally, pore sizes of 100 nm were reported by Haller according to Figure 2.12 with an alkali borosilicate glass heat treated at 680°C for 15 hours [76]. Similarly, Kobubu reported pore sizes between 80-139 nm for a $6Na_2O–25B_2O_3–69SiO_2$ glass heat treated at 650 °C for 14 to 63 hours [147].

It is also shown that within the range of heat treatment temperatures, the pore sizes of glasses with 3 mol% ZrO_2 have smaller values. Du et al. [126], reported that as ZrO_2 enters the silica structure, $[BO_4]^-$ groups are converted into $[BO_3]$ groups . Since three-coordinated boron units have a higher bond energy (119 kcal/mol) than four-coordinated boron units, once phase separation occurs, it is more difficult to break B-O-Si bonds from $[BO_3]$ than of $[BO_4]^-$ (increase in viscosity) [126]. Spinodal decomposition is slower because less concentration of boron is transferred to the soluble phase at the beginning of the process, and the growth rate by coarsening of the soluble phase is also inhibited [72].

Figure 4.19, indicates the increase of pore size with time of heat treatment. As more time is allowed in the spinodal phase separation, more borate will separate from the silica matrix, increasing its pore size. Other studies also show a similar results [64][127].

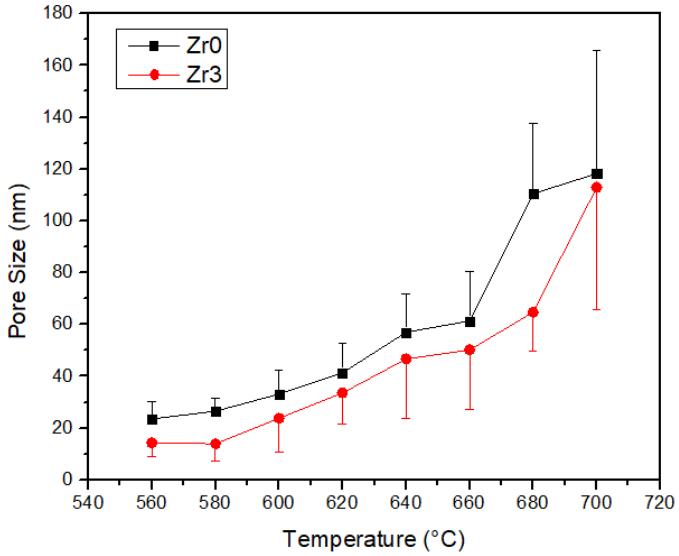

Figure 4.18: Influence of heat treatment temperature on the pore size of glasses with 0 and 3 mol% ZrO_2. The standard deviation is given by the bars in the diagram.

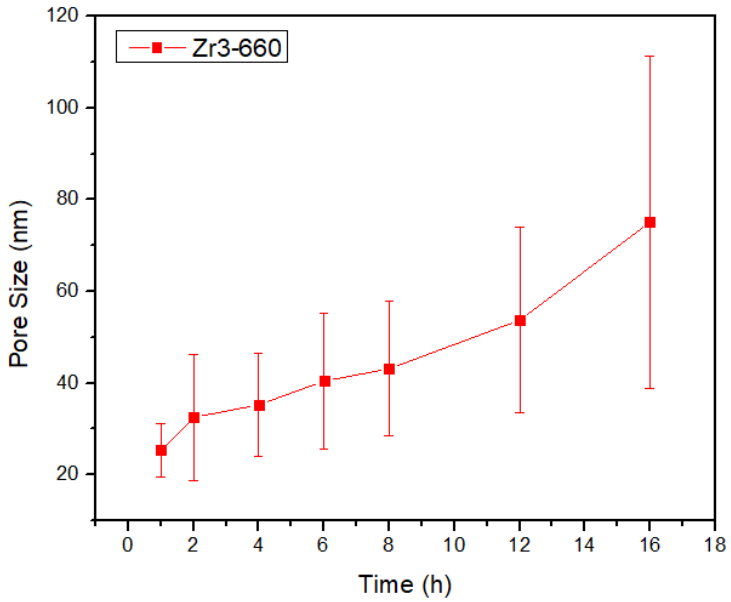

Figure 4.19: Influence of heat treatment time on the pore size of Zr3-660. The standard deviation is given by the bars in the diagram.

4.8. Leaching process

Different leaching parameters were taken into consideration on Zr0-680 and Zr3-680 glasses to obtain porous glass samples aiming to extract all the alkali-borate rich soluble phase. The tests were divided in 3 stages, as some serious difficulties appeared (cracking and sample breaking) during the leaching tests. Fully leached samples with mechanical stability were required for further investigations. The mass loss (%) of samples after leaching is used to quantify the degree of the soluble phase extraction. According to Hammel, a porous glass with a mass loss of around 25 % with 3 mol% of remaining boric oxide was achieved for a similar glass composition of $77SiO_2$-$18B_2O_3$-$5Na_2O$ [116].

4.8.1. Stage 1

Leaching with a 1 M HCl solution at room temperature (RT) for up to 16 hours was selected (see Figure 4.20). The mass loss increases with leaching time, however after 16 hours, mass loss values below 3 % were registered. Samples after leaching and drying at room temperature didn't present any cracks. The thickness of further samples tested were between 1.5 and 1.7 mm.

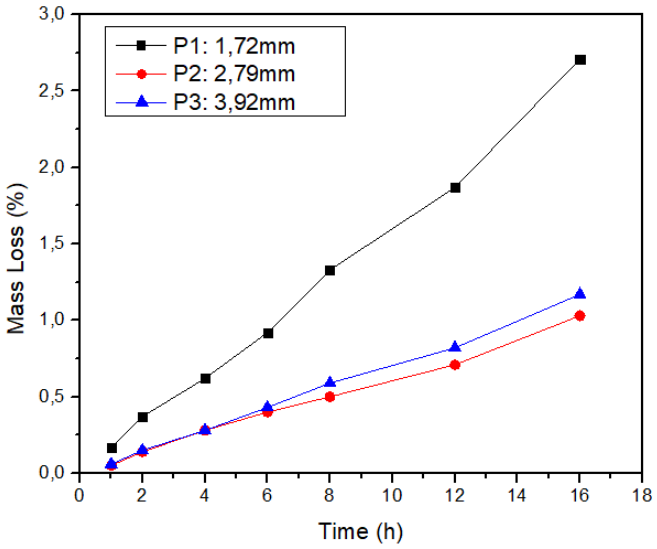

Figure 4.20: Mass loss of Zr3-680 samples heat treated for 12 hours and leached in 1 M HCl at RT, dried at RT. Thickness of the samples before leaching are shown in the diagram.

After 1 day of leaching (1 M HCl, RT) a mass loss of 3.5 % was registered as shown in Figure 4.21 but in this case the samples were dried after leaching in an oven at 90 °C. The samples showed a surface with flakes (see Figure 4.22).

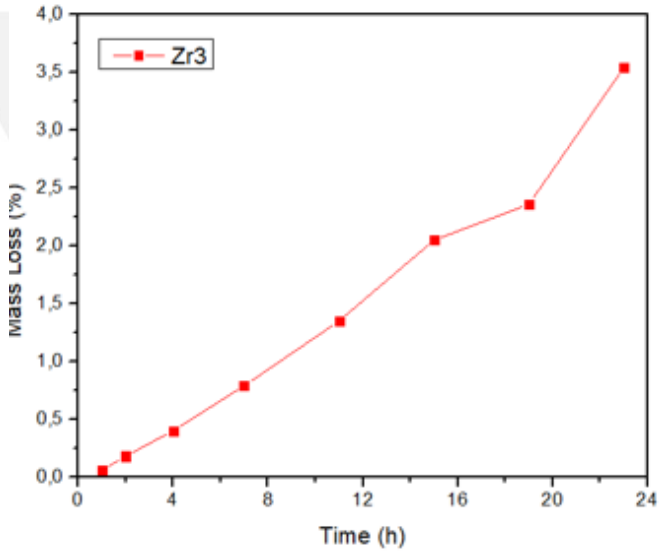

Figure 4.21: Mass loss of Zr3-680 samples heat treated for 12 hours and leached in 1 M HCl at RT, dried at 90 °C.

Figure 4.22: 1 M HCl RT leached sample Zr3-680 after drying at 90 °C. The glass surface shows flakes. The size of the sample is around 2x2 cm^2.

As literature suggests [92], increasing the leaching temperature promotes higher leaching rates. Similar parameters to previous test were chosen for the same heat treated glass (see Figure 4.23). Round samples of 1.5 cm diameter were leached in 1 M HCl for up to 26 hours at 60 °C and dried at room temperature. A mass loss of only 5.4 % is obtained. Glass samples didn't present any cracks.

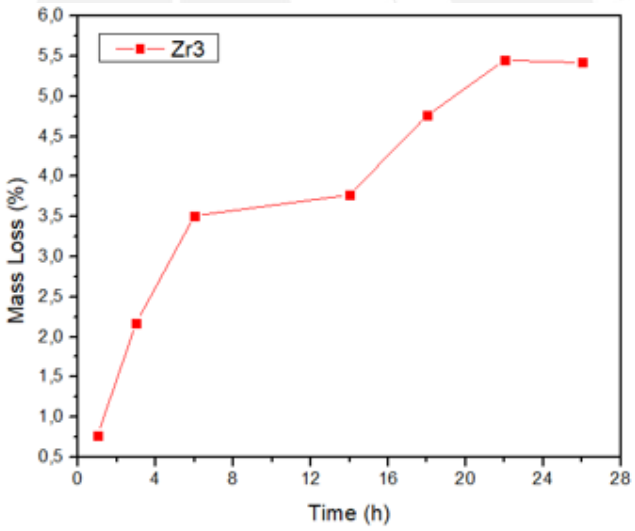

Figure 4.23: Mass loss of round Zr3-680 samples heat treated for 12 hours and leached in 1 M HCl at 60 °C, dried at RT.

Tests with longer periods of leaching time and higher leaching temperature were carried out (see Figure 4.24). Round samples leached at 60 °C for up to 5 days reached 13.5 % of mass loss but broke. Figure 4.25 shows the morphology of this leached sample. A thin layer on the leached surface is observed and it is possibly formed by the precipitation, from the solution, of the leached borate.

Since in this case, the same sample was used for consecutive leaching processes, the multiple temperature changes may have influenced the sample breaking. After 4 days of continuous leaching with similar mass loss, the sample didn't break. At 85 °C of leaching temperature, a 13.3 % mass loss was achieved after only one day without sample breaking, yet the sample broke after 2 days reaching 18.8 % mass loss.

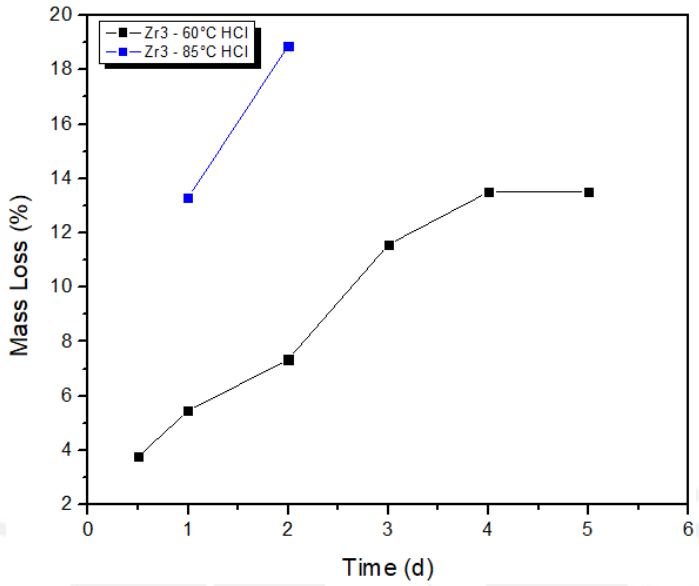

Figure 4.24: Mass loss of round Zr3-680 samples heat treated for 12 hours and leached in 1 M HCl at 60 °C (black) and 85 °C (blue), dried at RT.

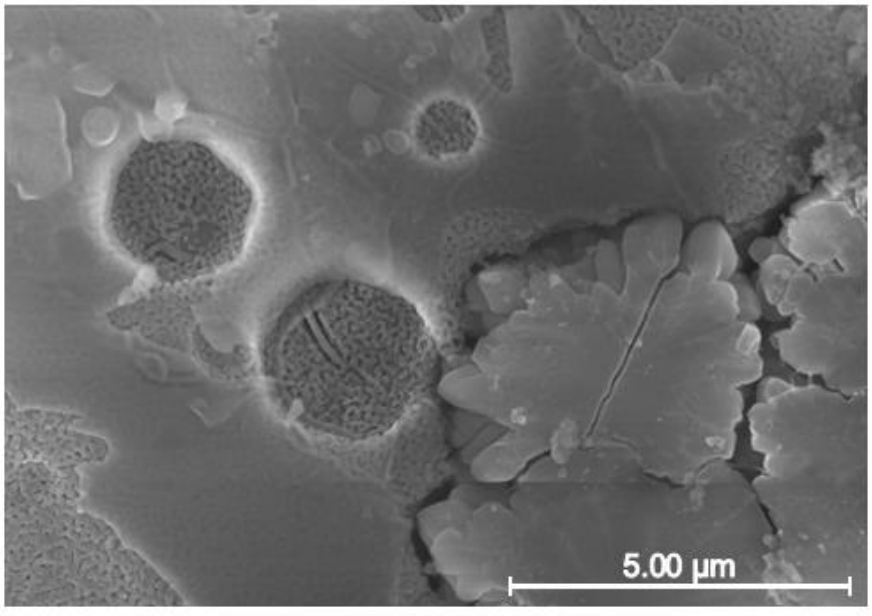

Figure 4.25: Morphology of a Zr3-680 sample leached in 1 M HCl solution at 60 °C for 5 days. A thin borate layer on the leached surface is observed.

Leaching test at room temperature and 60 °C on round Zr0-680 samples were carried out in 1 M HCl. At RT, 13.5 % mass loss is obtained after 1 day of leaching without sample breaking. With further leaching for up to 3 days, the sample broke but a mass loss around 20.7 % was registered. At 60 °C, 17 % mass loss was achieved but the sample broke after one day of leaching (see Figure 4.26).

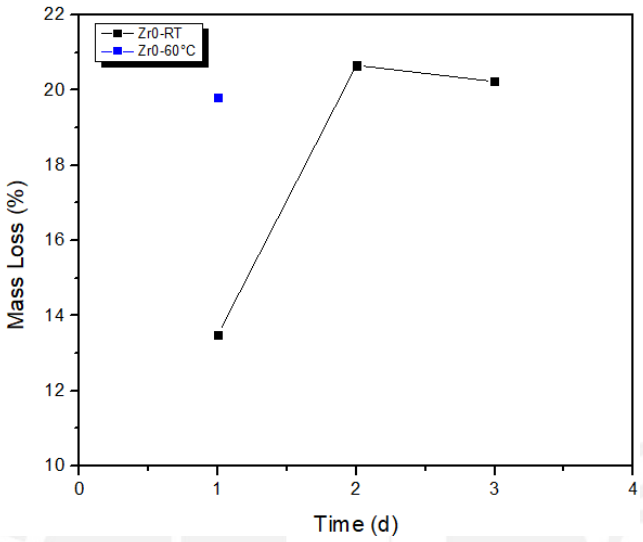

Figure 4.26: Mass loss of round Zr0-680 samples heat treated for 12 hours and leached in 1M HCl at RT (black) and 60 °C (blue), dried at RT.

4.8.2. Stage 2

To mitigate the sample breaking, 70 % ethanol was added to 1 M HCl solution in a 1 to 9 ratio. Surfactant agents are used to reduce the surface tension of the acid, decreasing the stress produced by capillary forces. Similar leaching parameters using surfactants were taken by Huang and Takamori et al. [109][117]. Figure 4.27 shows the mass loss of Zr3-680 samples leached at 70 °C for up to 13 days with a maximum mass loss of 17.84 %. All samples didn't break but presented cracks after leaching. After 9 days the mass loss values varied within the 17-18 % range. It can be inferred that a significant amount of borate phase had been extracted by this time. However, these values are still lower than the 25 % mass loss reported in literature [116]. This can be explained by the inhibition of the phase separation if zirconia is added. There is less amount of borate phase separated, thus the amount of mass loss during leaching is lower.

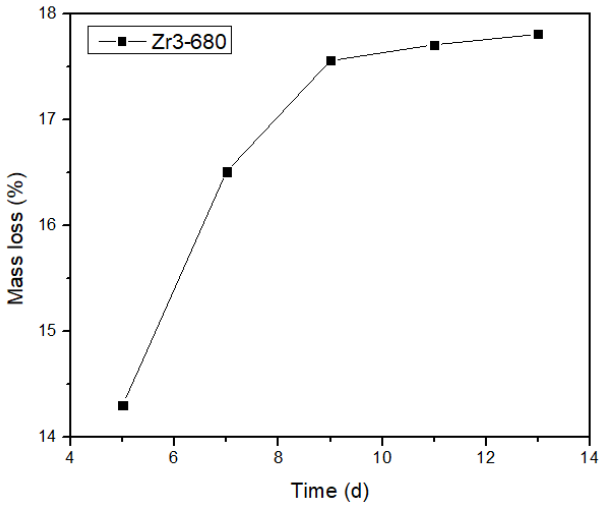

Figure 4.27: Mass loss of Zr3-680 samples heat treated for 12 hours and leached in 1 M HCl + 70 % ethanol (9:1 ratio) at 70 °C for up to 13 days, dried at RT.

The same leaching parameters were applied to square rod samples (20 x 3 x 3 mm). After 5 days of leaching, the mass loss obtained was 16.24 % and 16.56 % with minimal cracking in both samples. SEM images of the Zr3-680 samples show the depth of the leaching process. Figure 4.28a shows the cross section of the sample with a 67 µm fully leached layer on the surface. The fully leached region is shown in Figure 4.28b. Deeper in the sample, there is a semi-leached and a non-leached interface shown in Figure 4.28c and 4.28d.

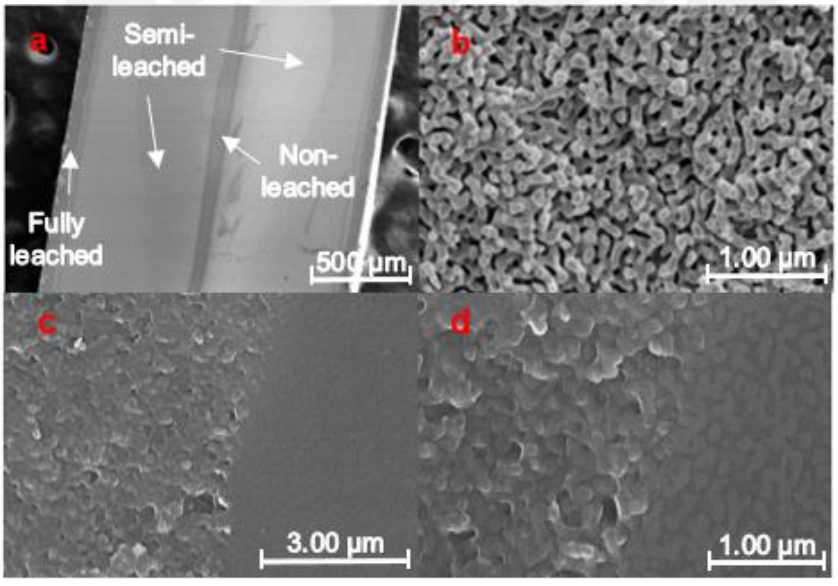

Figure 4.28: SEM images of Zr3-680 samples leached for 5 days in 1M HCl + 70 % ethanol at 70 °C, a) cross section of the sample showing the depth of leaching, b) morphology of the fully leached layer close to the surface and c) & d) interface between the semi-leached and a non-leached layers.

Taking into account the values of Zr0-680 leached at RT (Figure 4.26), new samples were leached at RT for two days to observe if the samples are stable enough to withstand the leaching process. Results are shown in Table 4.3. Values higher than 20 % mass loss could be related to sample breaking which didn't allow a proper mass loss calculation. Figure 4.29 shows the sample condition after 2 days of leaching. SEM images of sample 2 after 2 days of leaching show the cross section of the leached sample and its morphology in Figures 4.30a and 4.30b, respectively.

Table 4.3: Mass loss of Zr0-680 samples leached in 1 M HCl + ethanol at RT for up to 2 days, dried at RT.

Sample	Mass loss (%)	Condition
1	17.73	Broken
2	22.45	Broken
3	23.49	Broken
4	23.57	Broken
5	17.63	Not broken
6	19.70	Not broken
7	18.34	Not broken

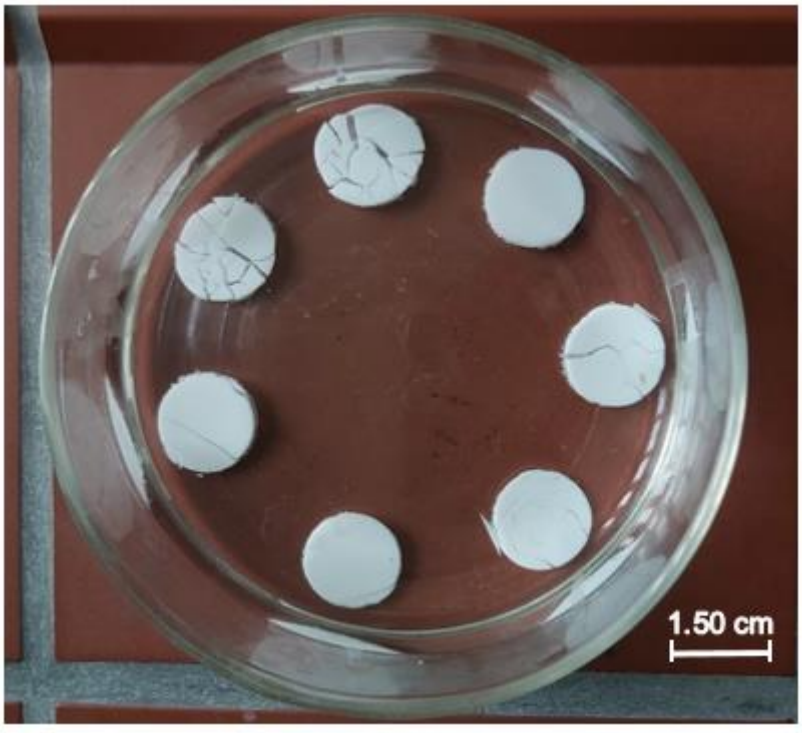

Figure 4.29: Zr0-680 samples condition after 2 days of leaching in 1 M HCl + ethanol at RT.

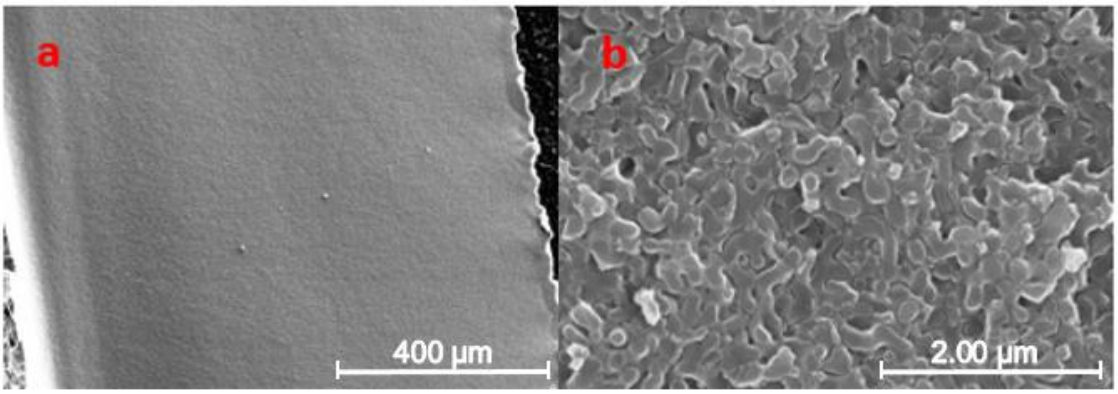

Figure 4.30: SEM images of Zr0-680 samples leached for 2 days in 1 M HCl + ethanol at RT, a) cross section of the leached sample and b) morphology of the fully leached layer close to the surface.

4.8.3. Stage 3

New samples were heat treated at 680 °C. This time, after phase separation the temperature was kept constant at 560 °C for 6 hours to promote the relieve of thermal stresses that may be causing cracking and breaking of the samples.

A solution of 2 M HCl + 70 % ethanol (ratio 9:1) at room temperature was used to leach Zr0-680 and Zr3-680 disc samples. Figure 4.31 shows the mass loss of Zr0-680 samples after for up to four days of leaching. A 24.7 % mass loss was reached.

This value is close the 25 % reported in literature [116]. The leached samples did not break in that case. It can be concluded that the additional heat treatment step at 560 °C increased the sample stability during the leaching process. For Zr3-680 glasses, the aim was to check if mass losses of 17-18 % from stage 2 can be surpassed. However, after 4 days of leaching with the same solution but at 70 °C, all samples broke. The increase in concentration of HCl could be a factor as it increases the amount of silica and zirconia gel in the pores [98]. In this type of glass, silica and zirconia gels are formed in the pore walls and channels, as explained in section 2.12. Blocking of the leaching process by agglomeration of gels can occur, leading to stress and crack formation in the structure [61].

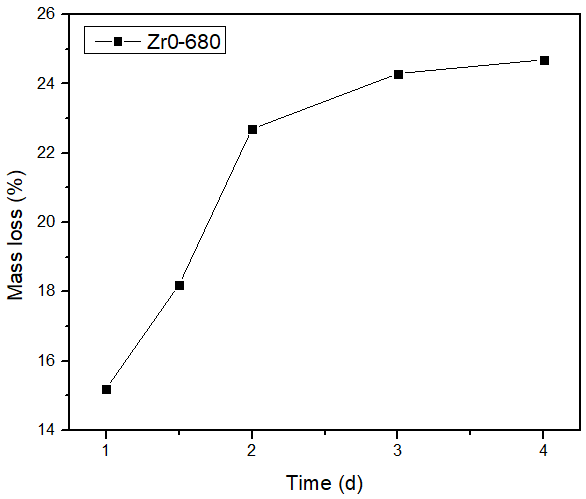

Figure 4.31: Mass loss of Zr0-680 samples heat treated for 12 hours and subsequently kept at 560 °C for 6 hours, leached in 2 M HCl + ethanol (ratio 9:1) at RT for up to 4 days, dried at RT.

4.9. Alkali resistance

Alkali resistance tests were carried out under 0.1 M NaOH solution (pH = 13) at RT for up to 22 hours. Figure 4.32 shows the results for Zr0-660 and Zr3-660 glasses leached in 1 M HCl at room temperature for 24 hours. Average mass losses of 18.22 % and 2.05 % for Zr0-660 and Zr3-660 were reported after the 22 hour test, respectively. According to previous results in stage 1, these glasses are not fully leached. With stage 1 acid leaching parameters, the borate phase mass losses for Zr0-660 and Zr3-660 are around 15 % and 5 %, respectively.

At 22 hours, in 3 mol% ZrO_2 glasses, the alkali resistance is improved approximately 10 times. Nakashima reported similar improvement if ZrO_2 and CaO were added to a $10Na_2O$-$25B_2O_3$-$65SiO_2$ glass [125].

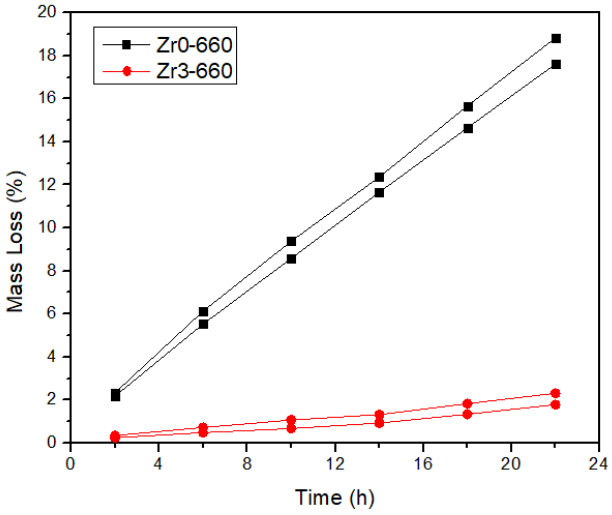

Figure 4.32: Influence of ZrO_2 addition on the mass loss in 0.1 M NaOH solution for Zr0-660 and Zr3-660 glasses. Two samples of each heat treated glass composition were tested.

Acid leaching of Zr0-680 and Zr3-680 glasses in 1 M HCl + ethanol solution (stage 2 parameters) resulted in an average borate phase mass loss of 19.03 % (2 days, RT) and 16.75 % (7 days, 70 °C), respectively. At 22 hours of alkali leaching, the average mass loss reached 19.8 % for Zr0-680 glasses. As shown in Fig. 4.33 a much lower mass loss after alkali attack is observed for the ZrO_2 containing glasses. The alkali resistance is improved 4 times if 3 mol% of ZrO_2 is added. This agrees with Kukizaki results, that stated an alkali durability increase of 3.5 times when 3.5 mol% ZrO_2 is added in a Na_2O-CaO-Al_2O_3-B_2O_3-SiO_2 system [43].

In both cases, the alkali resistance is improved by promoting the formation of Zr-O-Si, Si-O-Si covalent bonds and a higher number bridging oxygen which strengthen the silica structure preventing reactions with the silica network [43].

However, this effect is reduced (from 10 times to 4 times) in samples with higher leaching depth, therefore higher surface area. As Yazawa et al. reported, the formation of zirconia gel in the pores of zirconia containing glasses is feasible [64]. A certain amount of zirconia could also be phase separated away from the silica phase and extracted during leaching. This decreases the durability of glass against alkali solutions.

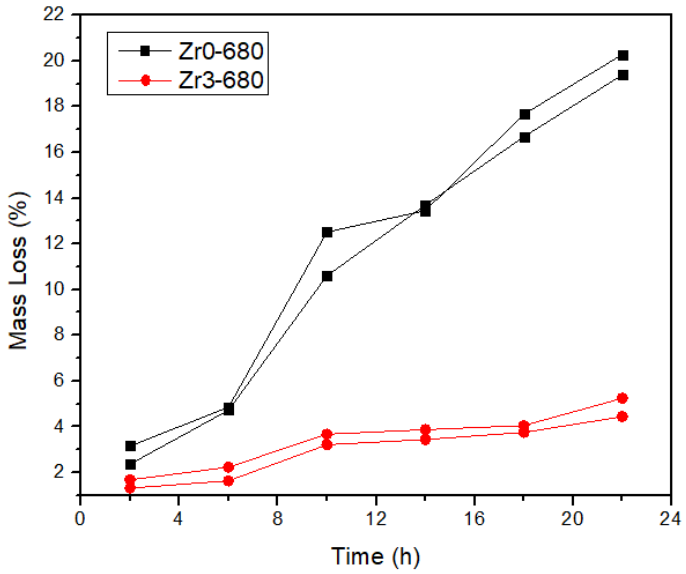

Figure 4.33: Influence of ZrO_2 addition on the mass loss in 0.1 M NaOH solution of Zr0-680 and Zr3-680 glasses. Two samples of each heat treated glass composition were tested.

CHAPTER 5

5. Conclusions

5.1. Glass characterization

Phase separation was successfully achieved for sodium borosilicate glasses with 0 and 3 mol% ZrO_2 heat treated between 560 and 700 °C. On the other hand, glasses with 6 mol% ZrO_2, heat treated from 600 to 660 °C, did not uniformly phase separate. According to SEM images, 0 and 3 mol% ZrO_2 samples showed an interconnected phase separated structure. 6 mol% ZrO_2 glasses didn't phase-separate properly. XRD analysis identified a phase named arkelite to have crystallized during heat treatment which may have caused the incomplete phase separation. However, Zr0-BG and Zr3-BG XRD patterns didn't show any diffraction peaks.

Differential scanning calorimetry (DSC) was used to examine the ZrO_2 effect on the glass transition temperature (T_g). Zr6-BG showed an increase in T_g (520 °C), this effect is caused by the formation of additional Si-O-Si bonds. For smaller additions of zirconia (Zr3-BG), T_g remains similar to Zr0-BG. A probable increase in T_g in this glass is most likely in the error range of the T_g measurement. A similar tendency was observed in the density values as Zr06-BG presents 4.4 % higher density than Zr0-BG. ATR analysis provided information about the borate and silicate groups with their vibrational modes present in investigated glasses. However, it was not sensitive enough to show structural changes due to the ZrO_2 incorporation.

SEM image analysis of leached glasses (1 M HCl for 24 hours) and pore size measurements according to the DIN EN ISO 13383 norm were carried out. Three main tendencies were found. Pore size increases as the heat treatment temperature increases due to a decrease in viscosity allowing more borate phase to phase separate. Zr0-700 and Zr3-700 glasses reached pore sizes of 120 and 100 nm, respectively. Throughout all heat treatment temperatures, the pore size of 3 mol% ZrO_2 glass remains smaller than for 0 mol% ZrO_2 glass. This can be attributed to the inhibition effect of ZrO_2 on the phase separation process. Pore sizes increase with longer times of heat treatment.

5.2. Porous glass fabrication

The aim of the leaching process is to obtain fully leached samples. Different acid leaching parameters were taken into consideration. As a reference according to literature, a 25 % mass loss is desirable.

In stage 1, only low values (3.0 % and 3.54 %) of borate phase mass loss for Zr3-680 samples were obtained with leaching in a 1 M HCl solution at room temperature. After sample cleaning with distilled water, samples were dried in an oven at 90 °C. Following this drying method the glass surface started to flake. This effect doesn't happen when drying takes place at room temperature.

An increase in the leaching temperature increases the leaching rate. Further tests were conducted at higher leaching temperatures but under these conditions the samples started to break during the leaching process. A Zr3-680 sample after leaching at 60 °C for up to 4 days with 13.5 % mass loss didn't break, however the mass loss obtained is still relatively low. A similar value was obtained if the temperature was increased to 85 °C, but in this case it only took one day to achieve a 13.3 % loss of mass. After a second day of leaching the sample broke. A Zr0-680 sample didn't break when leached at room temperature for 1 day reaching 13.5 % mass loss.

In stage 2, ethanol was added to the 1 M HCl leaching solution. For Zr3-680 samples leached for 13 days, 17.84 % mass loss was achieved but cracking was present in all samples. Zr0-680 samples leached for 2 days at room temperature that didn't break, showed an average of 18.6 % mass loss.

In stage 3, ethanol was added to a 2 M HCl leaching solution. Zr0-680 samples were leached at room temperature for up to 4 days without breaking showing 24.7 % mass loss, a value that is similar to the goal of this work. However, Zr3-680 samples frequently broke at 4 days of leaching at 70 °C with this leaching solution.

The leaching process presented continuing difficulties to obtain fully leached samples in good condition. In the case of Zr0-680 samples, stage 3 leaching and heat treatment parameters allowed to obtain mechanically stable samples free of cracks. An improvement in sample condition was observed for Zr3-680 samples if ethanol was added as samples didn't break, however, they presented cracks. The presence of cracks in the sample prevented to continue with further mechanical tests and to compare results with Zr0-680 samples and current porous polymeric membranes used commercially.

5.3. Alkali resistance

The formation of additional Si-O-Si and Zr-O-Si bonds as ZrO_2 is added to the glass, significantly improves the alkali resistance. For Zr3-660 leached glasses, the alkali durability is improved up to 10 times compared to zirconia free phase separated and leached glasses. A similar behavior is observed for Zr3-680 leached glass, as the alkali durability is 4 times better than for the Zr0-680 leached glass.

Glasses containing zirconia can be used as porous membranes in separation processes, as they can withstand cleaning cycles with NaOH after fouling processes. However, samples need to be mechanically stable as well, which was not accomplished in this research.

CHAPTER 6

6. Future work

For a better pore characterization, it is suggested to carry out N_2 adsorption-desorption or mercury porosimetry.

Results show an increase in mechanical stability of the samples if ethanol is added to the leaching solution and if an additional heat treatment step is added after phase separation to relieve thermal tensions. Increasing the concentration of ethanol as well as longer or multiple heat treatment steps are recommended. Addition of new compounds such as NaCl, KCl or NH_4Cl in HCl or other acids (HNO_3 and H_2SO_4) at leaching temperatures around 100 °C, as studied in literature, is suggested.

An analysis of the chemical composition of the residual porous glass is recommended to confirm the total extraction of the alkali-borate phase. Titration process of the acid solution after leaching can also indicate the amount of borate and sodium extracted from the glass.

Acid/glass ratios above 100 ml/g are desirable to eliminate silica gel from the pores. This can mitigate the probability of gel agglomeration causing stress in the sample and could prevent the formation of a layer on the sample.

To improve the alkali resistance, an alkaline earth oxide (CaO) can be added to the composition. CaO will contribute to retain zirconia in the silica phase during phase separation.

CHAPTER 7

7. Literature

[1] G. Lu and X. Zhao, *Nanoporous Materials : Science and engineering*, vol. 4. London: Imperial college press, 2004.

[2] F. Schüth, K. Sing, and J. Weitkamp, *Handbook of porous solids*. Weinheim: Wiley-VCH, 2002.

[3] N. Alsawaftah, W. Abuwatfa, N. Darwish, and G. Husseini, “A Comprehensive Review on Membrane Fouling: Mathematical Modelling, Prediction, Diagnosis, and Mitigation,” *Water*, vol. 13, no. 1327, pp. 1–37, 2021.

[4] A. Gul, J. Hruza, and F. Yalcinkaya, “Fouling and chemical cleaning of microfiltration membranes: A mini-review,” *Polymers (Basel).*, vol. 13, no. 6, pp. 846–871, 2021.

[5] J. Luo, A. S. Meyer, R. V. Mateiu, D. Kalyani, and M. Pinelo, “Functionalization of a membrane sublayer using reverse filtration of enzymes and dopamine coating,” *ACS Appl. Mater. Interfaces*, vol. 6, no. 24, pp. 22894–22904, 2014.

[6] B. Malczewska and A. Żak, “Structural Changes and Operational Deterioration of the UF Polyethersulfone (Pes) Membrane Due to Chemical Cleaning,” *Sci. Rep.*, vol. 9, no. 1, pp. 1–14, 2019.

[7] K. J. Howe and M. M. Clark, “Fouling of microfiltration and ultrafiltration membranes by natural waters,” *Environ. Sci. Technol.*, vol. 36, no. 16, pp. 3571–3576, 2002.

[8] D. Pyle, *Separation for biotechnology*. London: Elsevier applied science, 1990.

[9] R. Müller, N. Anders, J. Titus, and D. Enke, “Ultra-thin porous glass membranes - An innovative material for the immobilization of active species for optical chemosensors,” *Talanta*, vol. 107, pp. 255–262, 2013.

[10] W. James, S. Pucilowski, and E. Urruti, “Chemically durable porous glass with enhanced alkaline resistance,” US-Patent 2013/0017387 A1, 2013.

[11] A. Jungbauer, “Chromatographic media for bioseparation,” *J. Chromatogr. A*, vol. 1065, no. 1, pp. 3–12, 2005.

[12] J. Y. Tian, Z. L. Chen, Y. L. Yang, H. Liang, J. Nan, and G. B. Li, “Consecutive chemical cleaning of fouled PVC membrane using NaOH and ethanol during ultrafiltration of river water,” *Water Res.*, vol. 44, no. 1, pp. 59–68, 2010.

[13] A. Urbanowska and M. Kabsch-Korbutowicz, “The application of nanofiltration in NaOH solution regeneration after ultrafiltration membrane cleaning,” *Desalin. Water Treat.*, vol. 128, no. January 2018, pp. 70–78, 2018.

[14] Y. Jang, J. Kweon, M. Kang, J. Park, J. H. Jung, and J. Ryu, “Effects of sodium hydroxide cleaning on polyvinylidene fluoride fouled with humic water,” *Membr. water Treat.*, vol. 8, no. 2, pp. 149–160, 2016.

[15] A. Ahmad, M. Said, and A. W. Mohammad, “Optimization of NaOH as the cleaning of Polyethersulfone (PES) membrane fouled by Palm oil mill effluent,” in *The Third Basic Science International Conference*, 2013, pp. 2–5.

[16] J. G. Hooley, “the Kinetics of the Reaction of Silica With Group I Hydroxides,” *Can. J. Chem.*, vol. 39, no. 6, pp. 1221–1230, 1961.

[17] V. S. Molchanov, “Corrosion of glasses by solutions of various hydroxides,” *Inst. Silic. Chem. Acad. sicence USSR*, pp. 893–897, 1957.

[18] H. Maraghechi, F. Rajabipour, C. G. Pantano, and W. D. Burgos, “Effect of calcium on dissolution and precipitation reactions of amorphous silica at high alkalinity,” *Cem. Concr. Res.*, vol. 87, pp. 1–13, 2016.

[19] D. L. Morse and J. W. Evenson, “Welcome to the Glass Age,” *Int. J. Appl. Glas. Sci.*, vol. 7, no. 4, pp. 409–412, 2016.

[20] J. Shelby, *Introduction to Glass Science and Technology*, vol. 2. Cambridge: The Royal Society of Chemistry, 2005.

[21] K. J. Rao, *Structural Chemistry of Glasses*. Amsterdam: Elsevier Science and Technology Books, 2002.

[22] E. D. Zanotto and J. C. Mauro, “The glassy state of matter: Its definition and ultimate fate,” *J. Non. Cryst. Solids*, vol. 471, no. May, pp. 490–495, 2017.

[23] W. Zachariasen, “The atomic arrangement in glass,” *J. Am. Chem. Soc.*, vol. 196, no. 1, pp. 3841–3851, 1932.

[24] F. Puertas, M. Torres-Carrasco, and M. M. Alonso, “Reuse of urban and industrial waste glass as a novel activator for alkali-activated slag cement pastes: A case study,” in *Handbook of Alkali-Activated Cements, Mortars and Concretes*,

Woodhead Publishing Limited, 2015, pp. 75–109.

[25] H. Jabraoui, Y. Vaills, A. Hasnaoui, M. Badawi, and S. Ouaskit, “Effect of sodium oxide modifier on structural and elastic properties of silicate glass,” *J. Phys. Chem. B*, vol. 120, no. 51, pp. 13193–13205, 2016.

[26] J. Sestak and J. Mares, *Glassy, amorphous and nano-crystalline materials*, 1st ed. Dordrecht: Springer, 2011.

[27] G. N. Greaves and S. Sen, “Inorganic glasses, glass-forming liquids and amorphizing solids,” *Adv. Phys.*, vol. 56, no. 1, pp. 1–166, 2007.

[28] M. Edén, “NMR studies of oxide-based glasses,” *Annu. Reports Prog. Chem. - Sect. C*, vol. 108, pp. 177–221, 2012.

[29] W. Vogel, *Structure and crystallization of glasses*. Leipzig: Edition Leipzig, 1971.

[30] H. Mehrer, *Diffusion in solids*. Berlin: Springer-Verlag Berlin Heidelberg, 2007.

[31] R. A. Smith, “Boron in glass and glass making,” *J. Non. Cryst. Solids*, vol. 84, no. 1–3, pp. 421–432, 1986.

[32] M. Hubert and A. J. Faber, “On the structural role of boron in borosilicate glasses,” *Phys. Chem. Glas. Eur. J. Glas. Sci. Technol. Part B*, vol. 55, no. 3, pp. 136–158, 2014.

[33] W. Haller, D. H. Blackburn, F. E. Wagstaff, and R. J. Charles, “Metastable Immiscibility Surface in the System Na_2O-B_2O_3-SiO_2,” *J. Am. Ceram. Soc.*, vol. 53, no. 1, pp. 34–39, 1970.

[34] A. Paul, *Chemistry of Glasses*. New York: Chapman and Hall, 1982.

[35] O. N. Koroleva, L. A. Shabunina, and V. N. Bykov, “Structure of borosilicate glass according to raman spectroscopy data,” *Glas. Ceram. (English Transl. Steklo i Keramika)*, vol. 67, no. 11–12, pp. 340–342, 2011.

[36] D. Manara, A. Grandjean, and D. R. Neuville, “Structure of borosilicate glasses and melts: A revision of the Yun, Bray and Dell model,” *J. Non. Cryst. Solids*, vol. 355, no. 50–51, pp. 2528–2531, 2009.

[37] G. Lu, “Mechanical properties of porous materials,” *Met. Sci. Heat Treat.*, vol. 45, no. 11–12, pp. 441–444, 1999.

[38] P. S. Liu and G. F. Chen, “Characterization Methods,” in *Porous Materials*, Oxford: Elsevier, 2014, pp. 411–492.

[39] B. D. Zdravkov, J. J. Čermák, M. Šefara, and J. Janků, “Pore classification in the characterization of porous materials: A perspective,” *Cent. Eur. J. Chem.*, vol. 5, no. 2, pp. 385–395, 2007.

[40] J. Rouquerol and D. Avnir, “Recommendations for the characterization of porous solids,” *J. Sound Vib.*, vol. 66, no. 8, pp. 1739–1758, 1994.

[41] K. S. W. Sing, “Reporting physisorption data for gas / solid systems with Special Reference to the Determination of S,” *Pure Appl. Chem.*, vol. 54, no. 11, pp. 2201–2218, 1982.

[42] R. Rice, *Porosity of ceramics*. New York: CRC Press, 1998.

[43] M. Kukizaki, “Large-scale production of alkali-resistant Shirasu porous glass (SPG) membranes: Influence of ZrO_2 addition on crystallization and phase separation in Na_2O-CaO-Al_2O_3-B_2O_3-SiO_2 gl,” *J. Memb. Sci.*, vol. 360, no. 1–2, pp. 426–435, 2010.

[44] K. Izumi, M. Utiyama, and Y. Y. Maruo, “A porous glass-based KI/A-CD chip for ozone sensing: Improvement in the humidity response of the chip through optimizing reagent concentrations in the impregnation process,” *Sensors Actuators, B Chem.*, vol. 268, pp. 1–6, 2018.

[45] Y. Y. Maruo, “Measurement of ambient ozone using newly developed porous glass sensor,” *Sensors Actuators, B Chem.*, vol. 126, no. 2, pp. 485–491, 2007.

[46] K. Asanuma, K. Numata, and Y. Y. Maruo, “A colorimetric method for the measurement of ppb-level NO in exhaled air using porous glass analytical chips,” *Sensors and Actuators Reports*, vol. 2, no. 1, p. 100019, 2020.

[47] U. Schadeck, K. Kyrgyzbaev, T. Gerdes, M. Willert-Porada, and R. Moos, “Porous and non-porous micrometer-sized glass platelets as separators for lithium-ion batteries,” *J. Memb. Sci.*, vol. 550, no. November, pp. 518–525, 2018.

[48] T. and Mögelin, H., Yao, G., Zhong, H., dos Santos, A. R., Barascu, A., Meyer, R., Krenkel, S., Wassersleben, S., Hickmann, T., Enke, D., Turek and U. Kunz, “Porous glass membranes for vanadium redox-flow battery application - Effect of pore size on the performance,” *J. Power Sources*, vol. 377, no. October 2017, pp. 18–25, 2018.

[49] J. Zhang, X. Xu, H. Xiaolong, and Y. Guihua, “$LiFePO_4$/$NaFe_3V_9O_{19}$/porous glass nanocomposite cathodes for Li_+/Na_+ mixed-ion batteries,” *J. Mater. Chem. A*, vol. 3, no. 44, pp. 22247–22257, 2015.

[50] K. Kuraoka, Y. Chujo, and T. Yazawa, “Hydrocarbon separation via porous glass membranes surface-modified using organosilane compounds,” *J. Memb. Sci.*, vol. 182, no. 1–2, pp. 139–149, 2001.

[51] E. D. Safronsky, Y. O. Roizin, and E. Rysiakiewicz-Pasek, “Application of porous glasses for humidity control,” *Opt. Mater. (Amst).*, vol. 5, no. 3, pp. 217–220, 1996.

[52] A. Rafferty, R. Hill, B. Kelleher, and T. O’Dwyer, “An investigation of amorphous phase separation, leachability and surface area of an ionomer glass system and a sodium-boro-silicate glass system,” *J. Mater. Sci.*, vol. 38, no. 19, pp. 3891–3902, 2003.

[53] B.-K. Hoffmann, M, Kreft, S, Georgi, G, Fulda, G, Pohl, M, Seeburg, D, “Improved catalytic methane combustion of Pd/CeO_2 catalysts via porous glass integration,” *Appl. Catal. B Environ.*, vol. 179, pp. 313–320, 2015.

[54] C. Goepel, M., Kabir, H., Küster, R. Saraçi, E., Zeigermann, P., Valiullin, and P. Chmelik, “Improving mass-transfer in controlled pore glasses as supports for the platinum-catalyzed aromatics hydrogenation,” *Catal. Sci. Technol.*, vol. 5, no. 6, pp. 3137–3146, 2015.

[55] Y. Yang, G. Zhang, and W. Xu, “Facile synthesis and photocatalytic properties of Ag-AgCl-TiO_2/rectorite composite,” *J. Colloid Interface Sci.*, vol. 376, no. 1, pp. 217–223, 2012.

[56] M. Hasanuzzaman, A. Rafferty, M. Sajjia, and A.-G. Olabi, “Production and Treatment of Porous Glass Materials for Advanced Usage,” in *Reference Module in Materials Science and Materials Engineering*, no. 1, Amsterdam: Elsevier Ltd., 2016, pp. 1–13.

[57] S. S. Moosavi and P. Alizadeh, “Effect of acid leaching time on pore diameter and volume of porous hollow glass microspheres,” *Mater. Lett.*, vol. 167, pp. 98–101, 2016.

[58] S. Krenkel, “Anisotrope, hierarchische Strukturierung von nanoporösen Gläsern,” PhD thesis,Technische Universität Ilmenau, 2018.

[59] D. Enke, F. Janowski, and W. Schwieger, “Porous glasses in the 21st century-a short review,” *Microporous Mesoporous Mater.*, vol. 60, no. 1–3, pp. 19–30, 2003.

[60] T. Jin, K. Kuraoka, and T. Yazawa, “Preparation of surface modified porous membranes and their pervaporation properties,” *Desalination*, vol. 148, no. 1–3, pp. 17–18, 2002.

[61] M. Kukizaki and T. Nakashima, “Acid Leaching Process in the Preparation of Porous Glass Membranes from Phase-separated Glass in the Na_2O-CaO-MgO-Al_2O_3-B_2O_3-SiO_2 System,” *Membrane*, vol. 29, no. 5, pp. 301–308, 2004.

[62] M. Hasanuzzaman, A. Rafferty, and A. G. Olabi, “Effects of zircon on porous structure and alkali durability of borosilicate glasses,” *Ceram. Int.*, vol. 40, no. 1, pp. 581–590, 2014.

[63] W. Konijnendijk, “The structure of borosilicate glasses,” PhD thesis, Technische Hogeschool Eindhoven, 1975.

[64] T. Yazawa, H. Tanaka, K. Eguchi, and S. Yokoyama, “Novel alkali-resistant porous glass prepared from a mother glass based on the SiO_2-B_2O_3-RO-ZrO_2 (R = Mg, Ca, Sr, Ba and Zn) system,” *J. Mater. Sci.*, vol. 29, no. 13, pp. 3433–3440, 1994.

[65] M. Lenoir, A. Grandjean, Y. Linard, B. Cochain, and D. R. Neuville, “The influence of Si,B substitution and of the nature of network-modifying cations on the properties and structure of borosilicate glasses and melts,” *Chem. Geol.*, vol. 256, no. 3–4, pp. 316–325, 2008.

[66] H. Doweidar, “Consideration of the boron oxide anomaly,” *J. Mater. Sci.*, vol. 25, no. 1, pp. 253–258, 1990.

[67] D. R. Uhlmann and R. R. Shaw, “The thermal expansion of alkali borate glasses and the boric oxide anomaly,” *J. Non. Cryst. Solids*, vol. 1, no. 5, pp. 347–359, 1969.

[68] W. Vogel, *Glass Chemistry*. Berlin: Springer, 1985.

[69] S. A. H. Sander, M. Weiss, R. Denecke, D. Enke, and H. Roggendorf, “Long-Term Heat Treatment of Phase Separating Sodium Borosilicate Glass,” *Adv. Eng. Mater.*, vol. 21, no. 6, pp. 1–10, 2019.

[70] D. Neuville, L. Cornier, and D. Caurant, *From glass to crystal*. Les Ulis: EDP Sciences, 2017.

[71] B. R. Wheaton and A. G. Clare, “Evaluation of phase separation in glasses with the use of atomic force microscopy,” *J. Non. Cryst. Solids*, vol. 353, no. 52–54, pp. 4767–4778, 2007.

[72] T. Yazawa, K. Kuraoka, T. Akai, N. Umesaki, and W. F. Du, “Clarification of phase separation mechanism of sodium borosilicate glasses in early stage by nuclear magnetic resonance,” *J. Phys. Chem. B*, vol. 104, no. 9, pp. 2109–2116, 2000.

[73] R. Doremus, *Glass science*, 2nd ed. New York: John Wiley and Sons Inc., 1994.

[74] J. M. Arun Varshneya, *Fundamentals of inorganic glases*, 3rd ed. Amsterdam: Elsevier, 2019.

[75] M. Lewis, *Glasses and glass-ceramics*. New York: Chapman and Hall, 1989.

[76] W. Haller, “Material and method for performing steric separations,” US-Patent 3,549,524, 1970.

[77] Z. Zhou, M. C. Wang, J. Han, F. Xu, and X. Zhao, “Effect of heat treatment on $7Na_2O$-$23B_2O_3$-$70SiO_2$ glass,” *Ceram. Int.*, vol. 37, no. 6, pp. 1769–1773, 2011.

[78] E. B. Ertuş, “Production and characterization of hierarchically porous transparent glasses,” PhD thesis, Middle East Technical University, 2020.

[79] W. Gille, D. Enke, F. Janowski, and T. Hahn, “About the Realistic Porosity of Porous Glasses,” *J. Porous Mater.*, vol. 10, no. 3, pp. 179–187, 2003.

[80] S. A. Gevelyuk, I. K. Doycho, D. E. Lishchuk, and L. P. Prokopovich, “Linear extension of porous glasses with modified internal surface in humid environment,” *Opt. Appl.*, vol. 30, no. 4, pp. 605–611, 2000.

[81] E. Porai-Koshits, *Phase-separation phenomena in glasses*. New York: Consultants Bureau, 1968.

[82] H. Tanaka, T. Yazawa, K. Eguchi, H. Nagasawa, N. Matsuda, and T. Einishi, “Precipitation of colloidal silica and pore size distribution in high silica porous glass,” *J. Non. Cryst. Solids*, vol. 65, no. 2–3, pp. 301–309, 1984.

[83] D. Enke, F. Janowski, W. Gille, and W. Schwieger, “Structure and texture analysis of colloidal silica in porous glasses,” *Colloids Surfaces A Physicochem. Eng. Asp.*, vol. 187–188, pp. 131–139, 2001.

[84] V. A. Kreisberg and T. V. Antropova, “Changing the relation between micro- and mesoporosity in porous glasses: The effect of different factors,” *Microporous Mesoporous Mater.*, vol. 190, pp. 128–138, 2014.

[85] D. Enke, K. Otto, F. Janowski, W. Heyer, W. Schwieger, and W. Gille, “Two-phase porous silica: Mesopores inside controlled pore glasses,” *J. Mater. Sci.*, vol. 36, no. 9, pp. 2349–2357, 2001.

[86] B. Biliński and A. L. Dawidowicz, “Investigation of porous structure and surface properties of controlled porosity glasses,” *Colloids Surfaces A Physicochem. Eng. Asp.*, vol. 118, no. 1–2, pp. 149–160, 1996.

[87] V. A. Kreisberg, V. P. Rakcheev, and T. V. Antropova, “The relationship between micro- and mesoporous substructures upon removal of colloidal silica from porous glasses subjected to alkaline treatment,” *Colloid J.*, vol. 76, no. 2, pp. 161–169, 2014.

[88] H. A. Elbatal, M. A. Azooz, E. A. Saad, and M. S. Amin, “Corrosion behavior mechanism of borosilicate glasses towards different leaching solutions evaluated by the grain method and FTIR spectral analysis before and after gamma irradiation,” *Silicon*, vol. 10, no. 3, pp. 1139–1149, 2018.

[89] R. H. Doremus, “Diffusion-controlled reaction of water with glass,” *J. Non. Cryst. Solids*, vol. 55, no. 1, pp. 143–147, 1983.

[90] J. Sanguino Otero, “Obtención de nanofibras de carbono in situ en vidrios porosos,” PhD thesis, Univeridad complutense de Madrid, 2014.

[91] F. H. El-Batal, E. M. Khalil, Y. M. Hamdy, H. M. Zidan, M. S. Aziz, and A. M. Abdelghany, “FTIR spectral analysis of corrosion mechanisms in soda lime silica glasses doped with transition metal oxides,” *Silicon*, vol. 2, no. 1, pp. 41–47, 2010.

[92] M. Shimbo, “Leach-Out Process of Phase Separated Sodium Borosilicate Glass,” *J. Ceram. Assoc. Japan*, vol. 80, no. 923, pp. 277–284, 1972.

[93] T. H. Elmer, “Porous and Reconstructed Glasses,” *Eng. Mater. Handb. Vol. 4*, vol. 4, pp. 427–432, 1992.

[94] T. Hood, “Method of treating borosilicate glasses,” US-Patent 2,215,039, 1940.

[95] F. Devreux, A. Ledieu, P. Barboux, and Y. Minet, “Leaching of borosilicate glasses. II. Model and Monte-Carlo simulations,” *J. Non. Cryst. Solids*, vol. 343, no. 1–3, pp. 13–25, 2004.

[96] V. A. Kreisberg, V. P. Rakcheev, and T. V. Antropova, “Influence of the acid concentration on the morphology of micropores and mesopores in porous glasses,” *Glas. Phys. Chem.*, vol. 32, no. 6, pp. 615–622, 2006.

[97] V. A. Kreisberg, T. V. Antropova, and S. V. Kalinina, “Effect of the composition and conditions of the synthesis of porous glass on their micro- and mesoporous structures,” *Glas. Phys. Chem.*, vol. 40, no. 5, pp. 501–512, 2014.

[98] G. Toquer, C. Delchet, M. Nemec, and A. Grandjean, “Effect of leaching concentration and time on the morphology of pores in porous glasses,” *J. Non. Cryst. Solids*, vol. 357, no. 6, pp. 1552–1557, 2011.

[99] T. V. Antropova, I. N. Anfimova, and G. F. Golovina, “Influence of the composition and temperature of heat treatment of porous glasses on their structure and light transmission in the visible spectral range,” *Glas. Phys. Chem.*, vol. 35, no. 6, pp. 572–579, 2009.

[100] T. V. Antropova, “Kinetics of corrosion of the alkali borosilicate glasses in acid solutions,” *J. Non. Cryst. Solids*, vol. 345–346, no. October, pp. 270–275, 2004.

[101] H. Kawamura, N. Takusagawa, S. Taruta, and K. Kitajima, “Occurrence of bimodal pore structure and leaching process in the preparation of porous glass from fluorine containing sodium borosilicate glass,” *J. Ceram. Soc. Japan*, vol. 104, no. 3, pp. 179–184, 1996.

[102] D. Aboutaleb, J. Douglad, B. Safi, O. Jbara, and A. Iratni, “Phase separation and chemical durability in the SiO_2-B_2O_3-Na_2O (SBN) glass system,” *Asian J. Chem.*, vol. 24, no. 2, pp. 473–480, 2012.

[103] A. Makishima, J. D. Mackenzie, and J. J. Hammel, “The leaching of phase-separated sodium borosilicate glasses,” *J. Non. Cryst. Solids*, vol. 31, no. 3, pp. 377–383, 1979.

[104] T. V. Antropova, T. A. Tsyganova, G. P. Roskova, I. G. Kostyreva, I. G. Polyakova, and S. V. Medvedeva, “Some features of leaching of two-phase alkali borosilicate glass containing PbO,” *Glas. Phys. Chem.*, vol. 27, no. 2, pp. 175–181, 2001.

[105] M. Konon, T. Antropova, T. Kostyreva, I. Drozdova, and I. Polyakova, “Leaching of phase-separated glasses in Na_2O-B_2O_3-SiO_2-Fe_2O_3 system,” *Chem. Technol.*, vol. 67, no. 1, 2016.

[106] B. Procyk, D. Dorosz, P. Bieniarz, A. Zawada, and D. Höhne, “Influence of Al_2O_3, ZrO_2 and TiO_2 on the properties of the microporous glasses from the system Na_2O-B_2O_3-SiO_2,” *Glas. Sci. Technol.*, vol. 76, no. 3, pp. 110–117, 2003.

[107] T. A. Tsyganova, T. V. Antropova, O. V. Rakhimova, and T. G. Kostyreva, “Specific features of the formation of a porous structure in products of leaching of two-phase sodium borosilicate glasses in acid-salt solutions,” *Glas. Phys. Chem.*, vol. 33, no. 2, pp. 122–129, 2007.

[108] T. A. Tsyganova, T. V. Antropova, and O. V. Rakhimova, “Influence of the composition of alkali borosilicate glass and leaching solution on the structure of nanoporous glasses,” *Glas. Phys. Chem.*, vol. 34, no. 2, pp. 224–226, 2008.

[109] X. Huang, “Manufacture of porous glass,” *J. Non. Cryst. Solids*, vol. 112, pp. 58–63, 1989.

[110] T. Takamori and M. Tomozawa, “HCl leaching late and microstructure of phase-separated borosilicate glasses,” *J. Am. Ceram. Soc.*, vol. 61, no. 11–12, pp. 509–512, 1978.

[111] T. Takahashi, C. Go- Fua, Y. Ogura, and T. Kai, “Effect of alumina content on surface area and micropore distribution of porous glass prepared from borosilicate glass,” *Can. J. Chem. Eng.*, vol. 70, no. 3, pp. 604–607, 1992.

[112] K. Eguchi *et al.*, “Chemically durable porous glass and process for the manufacture thereof,” US-Patent 4,778,777, 1988.

[113] O. V. Rakhimova, T. A. Tsyganova, T. V. Antropova, and T. G. Kostyreva, “Spectrophotometric determination of molecular forms of silica in solution during the leaching of alkali borosilicate glasses,” *Glas. Phys. Chem.*, vol. 26, no. 3, pp. 303–306, 2000.

[114] M. V. Lyubavin, T. M. Burkat, and V. N. Pak, “Fabrication of silica membranes with controlled pore structure,” *Inorg. Mater.*, vol. 44, no. 2, pp. 203–206, 2008.

[115] H. P. Hood and M. E. Nord, “Treated borosilicate glass,” US-Patent 2,106,744, 1938.

[116] J. Hammel, “Method of forming micro-porous glass fibers,” US-Patent 3,650,721, 1972.

[117] T. Takamori, “Relaxation of Thermal Stress in Phase- Separated Borosilicate Glasses,” *J. Am. Ceram. Soc.*, vol. 59, no. 3–4, pp. 121–123, 1976.

[118] G. W. Scherer, “Dilatation of Porous Glass,” *J. Am. Ceram. Soc.*, vol. 69, no. 6, pp. 473–480, 1986.

[119] G. W. Scherer and M. G. Drexhage, “Stress in leached phase- separated glass,” *J. Am. Ceram. Soc.*, vol. 68, no. 8, pp. 419–426, 1985.

[120] X. Lu, L. Deng, and J. Du, “Effect of ZrO_2 on the structure and properties of soda-lime silicate glasses from molecular dynamics simulations,” *J. Non. Cryst. Solids*, vol. 491, no. March, pp. 141–150, 2018.

[121] B. A. Proctor and B. Yale, “Glass fibres for cement reinforcement,” *Math. Phys. Sci.*, vol. 294, no. 1441, pp. 427–436, 1980.

[122] B. Bergeron, L. Galoisy, P. Jollivet, and F. Angeli, “First investigations of the influence of IVB elements (Ti, Zr, and Hf) on the chemical durability of soda-lime borosilicate glasses,” *J. Non. Cryst. Solids*, vol. 356, no. 44–49, pp. 2315–2322, 2010.

[123] X. Lu, L. Deng, S. Kerisit, and J. Du, “Structural role of ZrO_2 and its impact on properties of boroaluminosilicate nuclear waste glasses,” *npj Mater. Degrad.*, vol. 2, no. 1, 2018.

[124] S. Morimoto, “Preparation of chemically durable porous glasses,” *Ceram. Soc. Japan*, vol. 4, no. 1, pp. 56–79, 1990.

[125] K. Nakashima, K. Noda, and K. Mori, “Time-temperature-transformation diagrams for borosilicate glasses and preparation of chemically durable porous glasses,” *J. Am. Ceram. Soc.*, vol. 80, no. 5, pp. 1101–1110, 1997.

[126] W. F. Du, K. Kuraoka, T. Akai, and T. Yazawa, “Effect of additive ZrO_2 on spinodal phase separation and pore distribution of borosilicate glasses,” *J. Phys. Chem. B*, vol. 105, no. 48, pp. 11949–11954, 2001.

[127] M. Hasanuzzaman, M. Sajjia, A. Rafferty, and A. G. Olabi, “Thermal behaviour of zircon/zirconia-added chemically durable borosilicate porous glass,” *Thermochim. Acta*, vol. 555, pp. 81–88, 2013.

[128] D. R. De Villiers, M. A. Res, and R. O. Heckroodt, “Alkali-resistant porous glass produced from a Na_2O-B_2O_3-Y_2O_3-ZrO_2 glass,” *J. Mater. Sci. Lett.*, vol. 5, no. 3, pp. 277–278, 1986.

[129] Y. Murakami, “Method of strengthening the alkali resistance of a porous glass,” US-Patent 4,661,138, 1987.

[130] W. Tomb, “Enzymes bound to carriers having a metal oxide surface layer,” US-Patent 3,783,101, 1974.

[131] H. J. Haugen and S. Bertoldi, “Characterization of morphology-3D and porous structure,” in *Characterization of Polymeric Biomaterials*, Elsevier Ltd., 2017, pp. 21–53.

[132] B. Yalcin, S. E. Amos, and J. Tangeman, “Characterization,” in *Hollow Glass Microspheres for Plastics, Elastomers, and Adhesives Compounds*, 2015, pp. 7–34.

[133] Q. Zheng, Y. Zhang, O. Gulbiten, J. C. Mauro, and E. D. Zanotto, “Understanding glass through differential scanning calorimetry,” *Chem. Rev.*, vol. 119, no. 13, pp. 7848–7939, 2019.

[134] J. Musgraves and H. Juejun, *Handbook fo glass*. Cham: Elsevier, 2019.

[135] J. Cline, “The optics and alignment of the divergent beam laboratory X-ray powder diffractometer and its calibration using NIST standard reference materials,” *Stand. News*, vol. 34, no. 2, pp. 57–61, 2006.

[136] K. Akhtar, S. A. Khan, S. B. Khan, and A. M. Asiri, “Scanning electron microscopy: Principle and applications in nanomaterials characterization,” in *Handbook of Materials Characterization*, 2018, pp. 113–145.

[137] W. Zhou, R. Apkarian, Z. L. Wang, and D. Joy, “Fundamentals of scanning electron microscopy (SEM),” *Scanning Microsc. Nanotechnol. Tech. Appl.*, pp. 1–40, 2007.

[138] A. Ausili, M. Sánchez, and J. C. Gómez-Fernández, “Attenuated total reflectance infrared spectroscopy: A powerful method for the simultaneous study of structure and spatial orientation of lipids and membrane proteins,” *Biomed. Spectrosc. Imaging*, vol. 4, no. 2, pp. 159–170, 2015.

[139] “Hochleistungskeramik - Mikrostrukturelle Charakterisierung - Teil 1: Bestimmung der Korngröße und der Korngrößenverteilung,” DIN EN ISO 13383-1, 2016.

[140] H. Darwish and M. M. Gomaa, “Effect of compositional changes on the structure and properties of alkali-alumino borosilicate glasses,” *J. Mater. Sci. Mater. Electron.*, vol. 17, no. 1, pp. 35–42, 2006.

[141] Z. Hou, S. Wang, and Z. Xue, “Crystallization and microstructural characterization of B2O3-Al2O3-SiO2 glass,” *J. Non. Cryst. Solids*, vol. 356, no. 4–5, pp. 201–207, 2010.

[142] M. Nolan, T. S. Perova, R. A. Moore, C. E. Beitia, J. F. McGilp, and H. S. Gamble, “Spectroscopic investigations of borosilicate glass and its application as a dopant source for shallow junctions,” *J. Electrochem. Soc.*, vol. 147, no. 8, p. 3100, 2000.

[143] T. G. V. M. Rao, A. Rupesh Kumar, K. Neeraja, N. Veeraiah, and M. Rami Reddy, “Optical and structural investigation of Eu^{3+} ions in Nd^{3+} co-doped magnesium lead borosilicate glasses,” *J. Alloys Compd.*, vol. 557, pp. 209–217, 2013.

[144] A. Yadav and P. Singh, “A review of the structures of oxide glasses by Raman spectroscopy,” *RSC Adv.*, vol. 5, no. 83, pp. 67583–67609, 2015.

[145] C. Gautam, A. K. Yadav, and A. K. Singh, “A Review on Infrared Spectroscopy of Borate Glasses with Effects of Different Additives,” *ISRN Ceram.*, vol. 2012, no. November, pp. 1–17, 2012.

[146] A. K. Singh and U. T. Nakate, “Microwave synthesis, characterization, and photoluminescence properties of nanocrystalline zirconia,” *Sci. World J.*, vol. 2014, 2014.

[147] Y. Kobubu and J. Chiba, “Porous glass, process for its production and glass material used for the production,” US-Patent 4,665,039, 1987.